Received: 23 October 2020 | Accepted: 10 July 2021

DOI: 10.1111/gbi.12464

ORIGINAL ARTICLE

gebiology WILEY

Messinian bottom-grown selenitic gypsum: An archive of microbial life

Marcello Natalicchio[1] | Daniel Birgel[2] | Francesco Dela Pierre[1] | Simone Ziegenbalg[3] | Lars Hoffmann-Sell[4] | Susanne Gier[5] | Jörn Peckmann[2]

[1]Dipartimento di Scienze della Terra, Università degli Studi di Torino, Torino, Italy

[2]Institut für Geologie, Centrum für Erdsystemforschung und Nachhaltigkeit, Universität Hamburg, Hamburg, Germany

[3]IFG Ingenieurbüro für Geotechnik, Bautzen, Germany

[4]Institut Dr. Nowak GmbH & Co. KG, Ottersberg, Germany

[5]Institut für Geologie, Universität Wien, Wien, Austria

Correspondence
Jörn Peckmann, Institut für Geologie, Centrum für Erdsystemforschung und Nachhaltigkeit, Universität Hamburg, 20146 Hamburg, Germany.
Email: joern.peckmann@uni-hamburg.de

Funding information
European Union's Horizon 2020 research and innovation programme under the Marie Skłodowska-Curie

Abstract

Primary gypsum deposits, which accumulated in the Mediterranean Basin during the so-called Messinian salinity crisis (5.97–5.33 Ma), represent an excellent archive of microbial life. We investigated the molecular fossil inventory and the corresponding compound-specific $\delta^{13}C$ values of bottom-grown gypsum formed during the first stage of the crisis in four marginal basins across the Mediterranean (Nijar, Spain; Vena del Gesso, Italy; Heraklion, Crete; and Psematismenos, Cyprus). All studied gypsum samples contain intricate networks of filamentous microfossils, whose phylogenetic affiliation has been debated for a long time. Petrographic analysis, molecular fossil inventories (hydrocarbons, alcohols, and carboxylic acids), and carbon stable isotope patterns suggest that the mazes of filamentous fossils represent benthic microbial assemblages dominated by chemotrophic sulfide-oxidizing bacteria; in some of the samples, the body fossils are accompanied by lipids produced by sulfate-reducing bacteria. Abundant isoprenoid alcohols including diphytanyl glycerol diethers (DGDs) and glycerol dibiphytanyl glycerol tetraethers (GDGTs), typified by highly variable carbon stable isotope composition with $\delta^{13}C$ values spanning from −40 to −14‰, reveal the presence of planktic and benthic archaeal communities dwelling in Messinian paleoenvironments. The compound inventory of archaeal lipids indicates the existence of a stratified water column, with a normal marine to diluted upper water column and more saline deeper waters. This study documents the lipid biomarker inventory of microbial life preserved in ancient gypsum deposits, helping to reconstruct the widely debated conditions under which Messinian gypsum formed.

KEYWORDS
archaea, Messinian, stratification, sulfate-reducing bacteria, sulfide-oxidizing bacteria

1 | INTRODUCTION

Primary bottom-grown gypsum is an excellent archive of ancient biosignatures (e.g., Schopf et al., 2012) and represents a promising target for understanding early life on Earth and for exploring the possibility of life on Mars (Allwood et al., 2013; Benison & Karmanocky, 2014). Fast growth of gypsum crystals allows for rapid entombment of organic material, including microalgae and prokaryotes, often the only fossils found in ancient marine evaporites (Dela Pierre et al., 2015; Schopf et al., 2012). A prominent archive is the primary

gypsum having accumulated in the Mediterranean Basin during the Messinian salinity crisis (MSC; 5.97–5.33 Ma; Roveri et al., 2014), when the Mediterranean was turned into the youngest salt giant of Earth history (e.g., Hsü et al., 1973). The Messinian gypsum deposits are grouped into three stratigraphic units (CIESM, 2008): the Primary Lower Gypsum unit, representing the first phase of the MSC (5.97–5.60 Ma); the Resedimented Lower Gypsum unit, consisting of large blocks of the Primary Lower Gypsum unit emplaced by gravity flows during the second phase of the MSC (5.60–5.55 Ma; Roveri et al., 2014); and the Upper Gypsum unit, deposited during the final phase of the crisis (5.55–5.33 Ma). The environmental conditions controlling the deposition of Messinian gypsum are still debated, especially due to the lack of modern analogs. The onshore Messinian primary gypsum deposits are largely composed of bottom-grown selenitic (i.e., larger than 2 mm and up to some meters in size) crystals. Among the best examples of bottom-grown laminated, selenite gypsum is the so-called "stromatolitic" gypsum deposits (*sensu* Rouchy & Monty, 2000 and Allwood et al., 2013) of Cyprus and Crete. Their formation has been explained by a combination of abiotic and microbially driven processes (cf. Allwood et al., 2013).

Intricate networks of filamentous microfossils (Dela Pierre et al., 2015; Panieri et al., 2010; Rouchy, 1982; Rouchy & Monty, 1981, 2000; Schopf et al., 2012; Vai & Ricci Lucchi, 1977), also described as "shoestring-" and "spaghetti-like" structures (Vai & Ricci Lucchi, 1977), are the most striking feature of many gypsum crystals. The phylogenetic affiliation of the microfossils has not been unequivocally determined. It was proposed that the filaments represent brine shrimp fecal pellets (Schreiber & Decima, 1976), algae (Vai & Ricci Lucchi, 1977), or cyanobacteria (Rouchy & Monty, 2000). An assignment to cyanobacteria was further substantiated on the basis of the extraction of 16*S r*RNA from fossiliferous gypsum of northern Italy (Panieri et al., 2010). Later on, Schopf et al. (2012) suggested that the filaments may rather represent the remains of colorless sulfide-oxidizing bacteria like *Beggiatoa* or *Thioploca*. The dense fossil accumulations have not resulted from settling of planktic filamentous organisms, but represent former benthic assemblages of microbial filaments (Dela Pierre et al., 2015). The recognition of abundant aggregates of microcrystalline pyrite and associated polysulfide—the latter representing a diagnostic criterion for this clade of bacteria—within the filaments agrees with the assignment of the filamentous fossils to the colorless sulfide-oxidizing bacteria (Dela Pierre et al., 2015). Based on this circumstance, an unequivocal identification of the phylogenetic affiliation of these microfossils would allow the reconstruction of the depositional environment of bottom-grown Messinian gypsum. Should the assignment to phototrophic cyanobacteria be correct, gypsum would have been deposited within the photic zone, that is, at a maximum depth of 200 m (Lugli et al., 2010). In contrast, colorless sulfide-oxidizing bacteria do not provide any depth constraints—these prokaryotes can live at any depth from bathyal to peritidal settings (Bailey et al., 2009)—but can shed light on the redox conditions at the seafloor and the presence of an active biogeochemical sulfur cycle in Messinian brines (cf. Schulz & Jørgensen, 2001).

The analysis of molecular fossils (lipid biomarkers) is a well-established approach to reconstruct the composition of microbial communities preserved in evaporites (e.g., Grice et al., 1998; Jahnke et al., 2004; Turich & Freeman, 2011). The rapid entrapment of lipids within evaporitic minerals tends to favor preservation for up to hundreds of millions of years (e.g., Schinteie & Brocks, 2017; Summons et al., 1999). Gypsum and microbial organosedimentary carbonate deposits are common sedimentary products of modern hypersaline settings (Aref & Taj, 2012; Dupraz et al., 2009; Petrash et al., 2012; Vogel et al., 2010). These deposits exhibit a typical molecular fossil association dominated by short-chain *n*-alkanes, fatty acids, and hopanoids, commonly including abundant cyanobacterial lipids (e.g., Bühring et al., 2009; Jahnke et al., 2014). In contrast to modern gypsum deposits, the molecular fossil inventory of the Messinian gypsum has only been rarely investigated and only some groups of lipids (i.e., *n*-alkanes, alkenones, and isoprenoids) have been used as proxies for paleoclimate (Vasiliev et al., 2017) or for paleoenvironmental reconstruction (Christeleit et al., 2015).

Here, we provide a comprehensive overview on the inventory of molecular fossils preserved in filament-bearing, primary bottom-grown selenitic gypsum formed during the first stage of the MSC in four marginal basins across the Mediterranean. The excellent preservation of molecular fossils, along with the determination of compound-specific carbon stable isotope compositions, enables us (1) to recognize the main groups of micro-organisms inhabiting Messinian aquatic ecosystems at times of gypsum formation and (2) to contribute to the identification of the enigmatic filamentous microfossils.

2 | GEOLOGICAL SETTINGS OF THE SAMPLED SECTIONS

Messinian primary gypsum from five sections was collected and analyzed for this study. The samples are from four Mediterranean peripheral basins, (1) the Nijar Basin (southeastern Spain) at the western margin of the Mediterranean, (2) the Vena del Gesso Basin (Italy; two sections) located in the northern sector of the Mediterranean, and the (3) Heraklion (Crete) and (4) Psematismenos (Cyprus) basins in the eastern Mediterranean (Figure 1). The studied samples are from various stratigraphic levels, but they share the presence of densely packed filamentous fossils.

2.1 | Nijar basin

The Nijar Neogene sedimentary succession fills a SW-NE elongated basin located in the internal zone of the Betic Cordillera (southeastern Spain; Fortuin & Krijgsman, 2003). The Messinian succession comprises (a) pre-MSC marine strata of the Abad Marls (a member of the Turre Formation; Van de Poel, 1991), (b) sulfate evaporites of the Yesares Formation (e.g., Fortuin & Krijgsman, 2003), which is considered as the local equivalent of the Mediterranean Primary

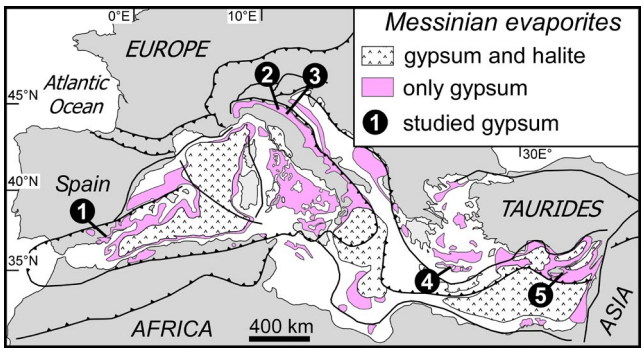

FIGURE 1 Distribution of Messinian evaporites in the Mediterranean and location of sampling areas (black dots). (1) Nijar Basin, SE Spain, (2,3) Vena del Gesso Basin (2: Monte Tondo quarry, 3: Monticino quarry), Italy, (4) Heraklion Basin, Crete, and (5) Psematismenos Basin, Cyprus. Modified after Rouchy and Caruso (2006)

Lower Gypsum unit (*sensu* Roveri et al., 2008), and (c) post-evaporitic continental and lagoonal deposits of the Feos Formation (Fortuin & Krijgsman, 2003; Omodeo Salé et al., 2012). The studied gypsum was sampled from the Yesares Formation exposed in the Gafares section (37°01′28″N, 1°59′17″W); here the Yesares Formation is approximately 70 m thick and consists of a cyclic alternation of at least eight gypsum and laminated marl couplets (Lu, 2006). The Gafares section starts with large selenitic gypsum crystals (the coarse and palmate twinned selenite facies of Lu, 2006) and shows an upward trend toward smaller gypsum crystals (grass-like selenite facies of Lu, 2006). The filament-rich selenitic gypsum was sampled at the base of the Yesares Formation. A dominantly marine origin has been suggested for the Yesares selenites based on $^{87}Sr/^{86}Sr$ ratios, trace element distribution, and the marine microfossil assemblages of the intercalated marls (Lu & Meyers, 2003; Lu et al., 2001, 2002).

2.2 | Vena del Gesso basin

The Vena del Gesso Basin is located in the northern Apennines (Italy), exposing a complete succession of the Primary Lower Gypsum unit along a ridge (Figure 2a). This succession consists of 16 cycles composed of gypsum and shale couplets (Lugli et al., 2010; Reghizzi et al., 2018; Vai & Ricci Lucchi, 1977), cut at the top by the Messinian erosional surface (Monticino quarry). The ideal cycle starts with bituminous shales, followed by stromatolitic limestones (Rouchy & Monty, 1981, 2000; Vai & Ricci Lucchi, 1977), which directly underlie the filament-bearing massive selenite facies (Figure 2b; Lugli et al., 2010). The size of the selenite crystals decreases upward, with the appearance of banded selenite and the branching selenite (the latter starting from the 6th cycle) facies completing an ideal cycle. Two samples of filament-bearing selenite gypsum were taken from the basal part of the third Primary Lower Gypsum cycle in the Monte Tondo quarry (44°15′04″N, 11°40′13″E) and from the second cycle in the Monticino quarry (44°13′29″N, 11°45′43″E).

2.3 | Heraklion basin

In the Neogene Heraklion Basin (central Crete), samples of filament-bearing gypsum were taken from the Tsangaraki section, approximately 1 km northeast of Profitis Ilias mountain (Allwood et al., 2013; Rouchy, 1982). Gypsum containing filaments was taken from dome-shaped bodies with stromatolitic morphology, the so-called "selenitic domical or columnar stromatolites" (Allwood et al., 2013). These deposits belong to the Lower Evaporites (Delrieu et al., 1993), which are the equivalent to the Primary Lower Gypsum. According to Rouchy (1982), they formed in a very shallow hypersaline lagoon. In the Tsangaraki area, the 2–3 m thick stromatolitic gypsum interval is located at the base of a gypsum unit (up to 80 m thick) containing different types of gypsum (selenite crystals, nodular and laminated gypsum, and gypsarenites). This unit overlies a chaotic interval of laminated fossiliferous carbonates and a rhythmic succession of laminated marls, diatomites, and fine-grained carbonates.

2.4 | Psematismenos basin

The Psematismenos Basin, located in the southeastern part of Cyprus, is a Neogene sedimentary basin surrounding the Troodos ophiolitic massif (Manzi et al., 2016). In this basin, Messinian evaporites comprise a thick gypsum unit resting on an alternation of pre-MSC sapropels, marls, and carbonate beds (Pakhna Formation). This gypsum unit has been subdivided in the western Polemi Basin into a Lower Gypsum, an Intermediate Breccia, and an Upper Gypsum subunit (Orszag-Sperber et al., 2009). The correlation of these subunits with the MSC chronostratigraphic model is still debated (Krijgsman et al., 2002; Manzi et al., 2016; Orszag-Sperber et al., 2009). According to Orszag-Sperber et al. (2009), in the Kalavasos area of the Psematismenos Basin only the Lower Gypsum is preserved and it correlates with the Primary Lower Gypsum unit of the western Mediterranean, representing the first phase of the MSC. Manzi et al. (2016), however, re-interpreted the Lower Gypsum subunit as an equivalent of the Resedimented Lower Gypsum unit, deposited during the second phase of the crisis (5.60–5.55 Ma; Roveri et al., 2014). The gypsum studied herein was collected in the Tokhni section (34°46′26″N, 33°18′54″E) and consists of selenitic filament-bearing gypsum with domal lamination (Figure 2c,d). According to Manzi et al. (2016), it represents a block of the Primary Lower Gypsum assigned to the Resedimented Lower gypsum unit.

3 | METHODS

Thin sections and thin platy gypsum crystals were studied with transmitted light on a Leica DM4500 P LED optical microscope equipped with a digital camera (Leica DFC 450 C). A FEI Inspect S equipped with an energy dispersive X-ray detection unit (EDAX Apollo XV) was used for scanning electron microscopy (SEM) and semi-quantitative element recognition. For SEM analyses, thin

gypsum slices were treated with deionized water to partly dissolve the selenitic gypsum. Mineralogical composition was determined with X-ray diffraction using a Panalytical X'Pert PRO diffractometer (CuKα radiation, 40 kV, 40 mA, step size 0.0167, 5 s per step; Table 1). The samples were loaded into the sample holders as oriented powder.

One representative gypsum sample from each location (approximately 200 g each) was selected for lipid biomarker analysis. The samples were carefully cleaned with acetone and ground with pestle and mortar to a fine powder. The extraction and separation procedure was carried out following Hoffmann-Sell et al. (2011). The powders were saponified in 6% KOH/MeOH (3 h, 80°C) and three times extracted with a microwave extraction system (MARS X, CEM Corporation) at 80°C and 300 W with dichloromethane (DCM):MeOH (3:1). The resulting total extracts were cleaned by separation into an *n*-hexane soluble fraction (maltenes) and a DCM-soluble fraction (asphaltenes). Maltene fractions were separated into four fractions of increasing polarity by column chromatography (hydrocarbons, ketones and esters, alcohols, carboxylic acids). In a second step, the remaining extracted gypsum powder was dissolved in clean water, enriched in NaCl, which had been annealed before, and subsequently extracted and fractionated as described above. The extracts of (1) gypsum powder (average 71 wt% of all extracted lipids) and (2) gypsum powder after dissolution (average 29% of all extracted lipids) yielded the same lipid distribution; for this reason, the total amount of identified compounds (Table 2) represents the sum of quantifications after both extractions.

For GC-MS analysis, alcohols were analyzed as their trimethylsilyl ether (TMS-) derivatives and carboxylic acids as their methyl ester (ME-) derivatives. Compounds from the hydrocarbon, alcohol, and fatty acid fractions were examined by gas chromatography flame ionization detection (GC-FID) and gas chromatography–mass spectrometry (GC–MS) using a Thermo Electron Trace DSQII GC–MS instrument at the MARUM, University of Bremen. Molecules were identified based on retention times and in comparison with published mass spectra. Contents are given in ng/g rock (dry weight). Compound-specific carbon isotope analysis (irm-GC/MS) was performed with a Thermo Electron GC-combustion-III-interface linked to a Thermo Electron Delta-plus XP mass spectrometer at the MARUM, University of Bremen. The $\delta^{13}C$ values of alcohols and carboxylic acids were corrected for the addition of trimethylsilyl and methyl derivatives, respectively. Each measurement was calibrated using several pulses of carbon dioxide gas with known composition at the beginning and the end of the run. The precision of measurements was checked with a mixture of *n*-alkanes (C_{15}–C_{29}) with known isotopic composition. The analytical standard deviation was smaller than 0.4‰.

Glycerol dibiphytanyl glycerol tetraethers (GDGTs) were prepared according to the procedure described in Hoffmann-Sell et al. (2011). An aliquot of each non-derivatized alcohol fraction was dissolved in *n*-hexane:propan-2-ol (99:1, v/v). Measurements were performed with high-performance liquid chromatography/atmospheric pressure ionization mass spectrometry (HPLC/ACPI-MS) using an Agilent 1200 series HPLC system coupled to an Agilent 6120A single quadrupole mass spectrometer at the MARUM, University of Bremen. Identification of GDGTs was obtained by screening m/z 400–1400. For GDGT peak integration, single ion monitoring (SIM) of the [M + H]+ions (m/z 1302, 1300, 1298, 1296, 1292) was used (dwell time 76 ms). Archaeol (m/z 654) was measured on both GC-FID and HPLC-APCI-MS and was used as reference compound. On the GC-FID, it was quantified with *n*-C_{19} alcohol as internal standard. The quantification of the GDGTs was carried out by correlating GC-FID and HPLC-APCI-MS data for each sample with archaeol. The response factors of archaeol and GDGT-0 on the HPLC-MS-APCI were 1.5 and 1.0, respectively.

4 | RESULTS

4.1 | Petrography and mineralogy

The studied gypsum samples show two types of morphologies: (1) decimeter-sized twinned selenite crystals (arrow-head or swallow-tail twins; Lugli et al., 2010) in the Vena del Gesso Basin (Figure 2b) and (2) decimeter-high stromatolitic build-ups made of gypsum (*sensu* Rouchy & Monty, 2000; Allwood et al., 2013) in Nijar, Crete, and Cyprus (Figure 2c,d). Both types of gypsum show an internal lamination, characterized by the alternation of mm thick turbid and limpid laminae (Figure 3a,b), possibly reflecting seasonal climate variability (Ortí, 2011; Dela Pierre et al., 2015; Reghizzi et al., 2018). In the limpid laminae, solid inclusions are scarce or even absent. In contrast, the turbid laminae entrap densely interwoven filamentous structures (Figures 3 and 4). In particular, in the twinned selenite crystals of the Monte Tondo and Monticino quarries, the filaments occur both in the re-entrant angles of the twins and along the vertical growth bands (Figure 3a), with their maximum lengths aligned to the main crystal faces. Clay-rich aggregates and sparse terrigenous grains are also observed in the turbid laminae. In gypsum build-ups (Nijar, Cyprus, Crete), the turbid laminae (light-colored in hand samples; Figure 2d) are 0.5–1 cm thick and contain dense aggregates (felts) of filaments aligned parallel to the laminae, while the limpid laminae (dark-colored in hand samples) contain much less filaments (Figure 3b). Accessory minerals like dolomite, celestine, and bassanite were detected in all the studied samples (Table 1).

The filaments are characterized by rounded ends and are up to 2 mm long and 60 to 110 μm across, with uniform width along their length (Figures 4 and 5a). Under transmitted light, the filaments appear as opaque tubular features (Figure 4b-g); some filaments are partially hollow (Figure 4c,d). The surface of the filaments is fluorescent when exposed to UV light (Figure 4e). Locally, the filaments contain small dolomite (e.g., in Monte Tondo and Nijar samples) and calcite (e.g., in Monticino, Crete, and Cyprus samples) crystals up to 15 μm in size (Figure 5b). Most filaments include aggregates of μm-sized opaque minerals (Figure 4e) identified as iron sulfide by SEM-EDAX.

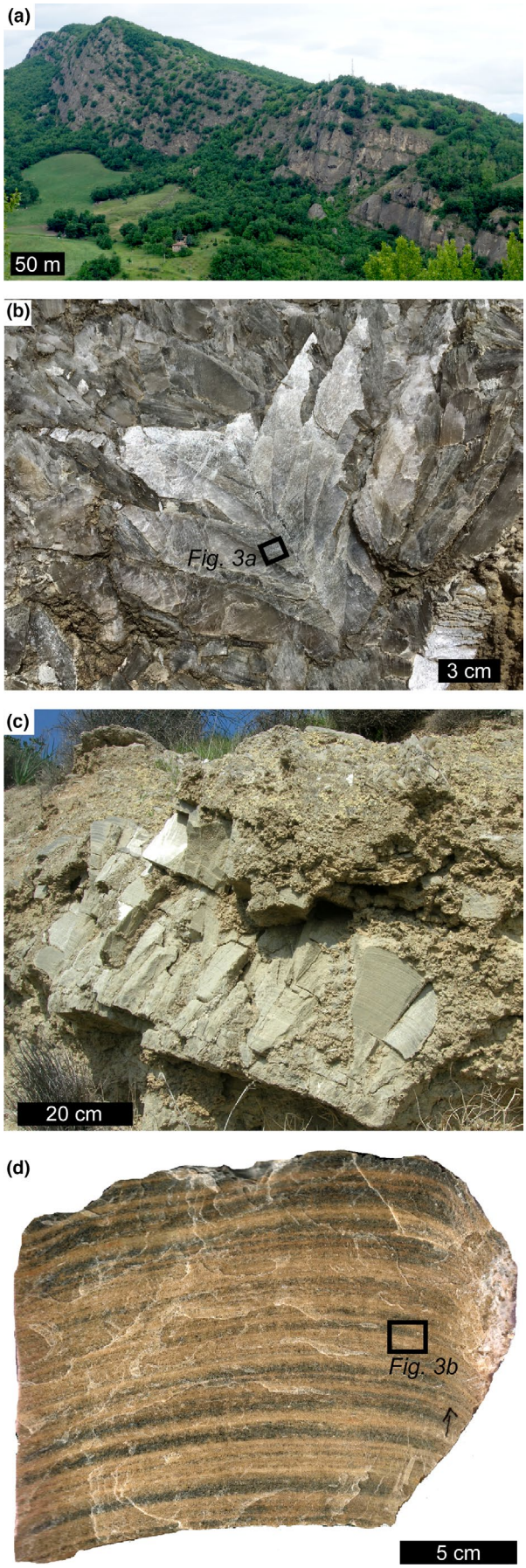

FIGURE 2 Messinian gypsum. (a) Panoramic view of the Vena del Gesso ridge made up of several tens of meters of thick gypsum beds (Primary Lower Gypsum unit). (b) Typical arrow-head selenitic crystal; note the darker re-entrant angle of the crystals (Monte Tondo, Italy). (c) Outcrop view of "gypsum stromatolites" (*sensu* Rouchy & Monty, 1981; Tokhni, Cyprus). (d) Close-up of laminated gypsum stromatolites (Tokhni, Cyprus)

4.2 | Lipid biomarker inventory

The lipid biomarker inventory is largely similar among the various studied samples (see Table 2), although some differences can be recognized. Generally, the western and northern Mediterranean samples (Nijar and Vena del Gesso) show lower total molecular fossil contents, ranging from 1,594 ng/g rock (Monticino) to 3,348 ng/g rock (Nijar). In contrast, the samples from the eastern Mediterranean (Crete and Cyprus) are typified by higher contents (up to 5,179 ng/g rock in the Crete sample; Table 2; Figure 6a). Carboxylic acids are the most abundant molecular fossils, representing more than 60 wt% of the total amount of lipids (Figure 6a).

4.2.1 | Hydrocarbons

The average contents of hydrocarbons range from *ca.*120 ng/g rock in the Monte Tondo and Monticino samples to *ca.* 420 ng/g rock in Nijar, Crete, and Cyprus. The *n*-alkanes are the dominant compounds in the hydrocarbon fractions, peaking either at *n*-C_{18} or *n*-C_{31}. Some variations in the distribution of short-chain (*n*-C_{17-21}) and long-chain (*n*-C_{26-33}) *n*-alkanes are observed. While Nijar, Crete, and Cyprus samples are characterized by prevailing short-chain *n*-alkanes, the Vena del Gesso samples show equal contents of short- and long-chain *n*-alkanes (Table 2). Among the short-chain *n*-alkanes, the *n*-C_{17} alkane is not enriched compared to neighboring *n*-alkanes, representing 8 to 11% of all hydrocarbons. The head-to-tail linked C_{19} isoprenoid pristane and the head-to-tail linked C_{20} isoprenoid phytane are the only isoprenoid hydrocarbons detected.

4.2.2 | Alcohols

Gypsum from all study sites contains *n*-alcohols, although in different proportions; short-chain *n*-alcohols comprise 16% of the alcohol fraction in Crete and Cyprus samples and about 57 and 55% in Nijar and Monte Tondo samples, respectively. Among all fractions, the molecular fossil inventories vary most from site to site for the alcohol fractions. While in the Nijar sample, the *n*-alcohols peak at *n*-C_{16}, *n*-C_{18} is most abundant in the Monte Tondo sample. In the Cyprus sample, *n*-C_{24} is most prominent. Apart from *n*-alcohols, isoprenoid alcohols account for 20% (Nijar) to 63% (Crete) of the compound inventory of the alcohol fractions, also including diphytanyl glycerol diethers (DGDs), glycerol dibiphytanyl glycerol tetraethers (GDGTs),

TABLE 1 Mineralogy of studied gypsum samples with entrapped filaments

Location	Mineralogy revealed by XRD	Additional mineral phases revealed by SEM/EDAX
Nijar	Gypsum, traces of dolomite	Celestine
Monte Tondo	Gypsum, traces of dolomite	Celestine, clay minerals
Monticino	Gypsum	Celestine, dolomite, calcite, clay minerals
Crete	Gypsum, traces of bassanite	Celestine
Cyprus	Gypsum	Celestine

the C_{20} isoprenoid phytanol, and *sn*2- and *sn*3-phytanylglycerol monoethers (ph-monoether; Figure 6b). Among the DGDs, the $C_{20\text{-}20}$ isoprenoid archaeol is the major isoprenoid alcohol in all sites with contents varying between 18 ng/g rock (Monticino) and 289 ng/g rock (Crete). In the Crete sample, $C_{20\text{-}20}$ archaeol is the most abundant compound representing 26% of all alcohols. Except for the Monticino sample, $C_{20\text{-}20}$ archaeol is always accompanied by $C_{20\text{-}25}$ archaeol (extended archaeol), yielding contents as high as 21 ng/g rock (Crete). All samples contain GDGTs with a very uniform distribution (Figure 6c). The GDGT with 4 cyclopentane and one cyclohexane moiety (GDGT-5, crenarchaeol; Table 2; Figure 6) predominates in all samples, comprising 40–50% of all GDGTs (Table 2). This compound is accompanied by minor amounts of the crenarchaeol isomer (crenarchaeol; Liu et al., 2016; Sinninghe Damsté et al., 2018). The acyclic GDGT (GDGT-0, caldarchaeol) varies between 15 and 31% of all GDGTs. GDGT-0 is accompanied by almost equal amounts of GDGTs with 1–2 cyclopentane moieties (GDGT-1; GDGT-2) and minor amounts of GDGT with 3 cyclopentane moieties (GDGT-3; Figure 6c).

Phytanol accounts for 2 to 5% of all the isoprenoid alcohols in samples from Nijar, Monte Tondo, and Cyprus, but was absent in the Monticino sample. Phytanol accounts for 20% in Crete and is accompanied by *sn*2- and *sn*3-ph-monoethers accounting for of 10 and 2% of all isoprenoid alcohols, respectively. Traces of these phytanyl monoethers are also present in Cyprus (*ca*. 2%). Further compounds in the alcohol fractions are cholesterol and dinosterol in all samples. Dinosterol is particularly abundant in the Nijar sample (5% of all alcohols) and in the Cyprus sample (9% of all alcohols). Traces of the pentacyclic triterpenoid tetrahymanol as well as cholestanol were only detected in samples from the eastern Mediterranean (Crete and Cyprus). The latter samples also contain low amounts (*ca*. 3% of the alcohols) of the C_{16} monoalkyl glycerolether (MAGE *n*-$C_{16:0}$).

4.2.3 | Carboxylic acids

Saturated short-chain *n*-fatty acids are the predominant components, accounting for 72 to 89% of the carboxylic acid fractions (Figure 6d). The *n*-C_{16} fatty acid is the major compound in all samples, representing 34–53% of all carboxylic acids, followed by *n*-C_{18} and *n*-C_{26} fatty acids. The terminally branched *iso*- and *anteiso*-$C_{15:0}$ and $C_{17:0}$ fatty acids are present with low contents (*ca*. 1 to 2%) in samples from Nijar, Crete, and Cyprus. Furthermore, monounsaturated *n*-$C_{18:1}$ is present in all samples (between 3 and 7% of all fatty acids) except for the Monte Tondo sample. Fatty acid *n*-$C_{16:1}$ was found only in the Nijar sample, accounting for 5% of all carboxylic acids.

4.3 | Compound-specific carbon stable isotopes

A synthesis of the compound-specific $\delta^{13}C$ values obtained from the studied gypsum samples is shown in Figure 7. The $\delta^{13}C_{hydrocarbon}$ values vary from −33 to −25‰. Long-chain *n*-alkanes are slightly more ^{13}C-depleted (−33 to −28‰) than short-chain *n*-alkanes (−29 to −24‰). Besides long-chain *n*-alkanes, pristane and phytane are among the most ^{13}C-depleted compounds with $\delta^{13}C$ values as low as −33‰. The *n*-alcohols show in general about 4‰ higher values than the *n*-alkanes. The isoprenoidal alcohols (phytanol, phytanyl monoethers, and DGDs) yielded the highest $\delta^{13}C$ values ranging from −22 to −13‰. Among them, the DGDs show a narrower range of values between −20 and −14‰. Relatively high values were also obtained for tetrahymanol and the MAGE in the Cyprus (−12 and −18‰, respectively) and Crete samples (−18 and −17‰). The $\delta^{13}C$ values of sterols range from −24 to −17‰, with the highest value found for dinosterol in Cyprus and Monticino samples (−17‰).

Among the carboxylic acids, $\delta^{13}C$ values were only obtained for few compounds. As for the *n*-alcohols, the *n*-fatty acids yielded about 4‰ higher values than the *n*-alkanes; only in the Crete sample, $\delta^{13}C$ values of *n*-fatty acids are in the same range like *n*-alkanes. The $\delta^{13}C$ values of the predominant short-chain *n*-alkanes range from −30 to −22‰. Only few data were obtained for monounsaturated *n*-$C_{16:1}$ (−26‰; Nijar) and *n*-$C_{18:1}$ fatty acids (−25 and −28‰ for Monticino and Crete, respectively), the terminally branched *iso*-$C_{17:0}$ fatty acid (−15‰; Crete), and phytanic acid (−16‰; Crete). The terminally branched *iso*-$C_{17:0}$ fatty acid and phytanic acid yielded similarly high values like the isoprenoidal alcohols.

5 | DISCUSSION

Modern marine gypsum deposits typically form in shallow-water hypersaline environments, including coastal mudflats (sabkhas), lagoons, and human-made salterns. In such settings, biological diversity is limited by high salinity (>110 PSU), which is lethal for most eukaryotes; consequently, these environments are inhabited by highly specialized prokaryotes, such as cyanobacteria and halophilic

TABLE 2 Molecular fossil inventory and compound-specific carbon isotopes of the Messinian gypsum with entrapped filaments

	Nijar		Monte Tondo		Monticino		Crete		Cyprus	
	ng/g rock	$\delta^{13}C$ [‰]	ng/g rock	$\delta^{13}C$ [‰]	ng/g rock	$\delta^{13}C$ [‰]	ng/g rock	$\delta^{13}C$ [‰]	ng/g rock	$\delta^{13}C$ [‰]
Hydrocarbons										
n-C_{17}	44	−25	13	−28	8	−27	30	−25	35	−26
n-C_{18}	63	−27	17	−29	12	−28	38	−28	39	−28
∑ sc-alkanes (*n*-C_{17-21})	231	−28 to −25	56	−30 to −28	40	−29 to −27	250	−29 to −27	159	−28 to −24
∑ lc-alkanes (*n*-C_{26-33})	169	−30 to −28	60	−32 to −31	32	−32 to −31	182	−32 to −30	110	−30 to −28
∑ *n*-alkanes	400		116		72		432		269	
Pristane	40	−29	16	−30	7	−31	26	n.d.	18	n.d.
Phytane	60	−30	17	−33	8	−33	4	−31	22	−30
∑ hydrocarbons	500		149		87		462		309	
Alcohols										
n-C_{16}	132	−27	88	−29	n.d.	n.d.	115	−23	54	−22
n-C_{18}	87	−29	259	−29	n.d.	n.d.	62	−29	49	−26
∑ sc-alcohols (*n*-C_{14-20})	350	−29 to −21	375	n.d.		n.d.	248	n.d.	181	n.d.
∑ lc-alcohols (*n*-C_{26-28})	35	−27 to −20	46	n.d.	35	n.d.	66	n.d.	126	n.d.
∑ *n*-alcohols	385		421		35		314		307	
MAGE *n*-$C_{16:0}$	0	n.d.	0	n.d.	0	n.d.	28	−17	23	−18
Phytanol	20	−14	14	−21	0	n.d.	220	−16	36	−13
*sn*2-phytanyl monoether	0	n.d.	0	n.d.	0	n.d.	108	−17	16	−22
*sn*3-phytanyl monoether	0	n.d.	0	n.d.	0	n.d.	35	−16	16	−20
Archaeol	54	−16	91	−20	18	−17	289	−18	124	−14
Extended archaeol	10	−15	18	−18	0	n.d.	21	−19	19	−15
Tetrahymanol	0	n.d.	0	n.d.	0	n.d.	5	−18	11	−12
Cholesterol	12	−19	56	−23	58	−22	26	−21	0	−24
Cholestanol	0	n.d.	0	n.d.	0	n.d.	37	−19	26	−21
Dinosterol	26	−19	0	−23	5	−17	9	−24	61	−17
GDGT-0 (caldarchaeol)	4		12		5		5		11	
GDGT-1	2		6		2		6		3	

(Continues)

TABLE 2 (Continued)

	Nijar		Monte Tondo		Monticino		Crete		Cyprus	
	ng/g rock	$\delta^{13}C$ [‰]	ng/g rock	$\delta^{13}C$ [‰]	ng/g rock	$\delta^{13}C$ [‰]	ng/g rock	$\delta^{13}C$ [‰]	ng/g rock	$\delta^{13}C$ [‰]
GDGT-2	4		7		2		4		4	
GDGT-3	1		4		0.5		4		2	
Crenarchaeol	9		34		10		14		15	
Crenarchaeol isomer	1		5		0.5		1		1	
Sum GDGTs	21		68		19		34		36	
∑ isoprenoid alcohols	105		191		37		707		247	
∑ alcohols	528		668		135		1,126		675	
Carboxylic acids										
n-$C_{15:0}$	120	−24	40	−28	52	−23	129	−25	156	−22
n-$C_{16:0}$	839	−26	715	n.d.	725	−25	1,229	−30	1,137	−25
n-$C_{17:0}$	65	−22	0	n.d.	48	n.d.	166	−25	219	−22
n-$C_{18:0}$	301	−24	258	n.d.	229	−26	434	−26	505	−23
n-$C_{26:0}$	151	n.d.	307	n.d.	27	−28	438	−28	317	−28
sc-fatty acids (*n*-C_{14-19})	1,795	−26 to −22	1,065	n.d.	1,226	n.d.	2,574	n.d.	2,629	n.d.
lc-fatty acids (*n*-C_{26-30})	172	n.d.	332	n.d.	49	n.d.	485	n.d.	356	n.d.
∑ *n*-fatty acids	1,967		1,397		1,275		3,059		2,985	
i-$C_{15:0}$	33	n.d.	0	n.d.	0	n.d.	47	n.d.	39	n.d.
ai-$C_{15:0}$	36	n.d.	0	n.d.	0	n.d.	47	n.d.	30	n.d.
i-$C_{17:0}$	25	n.d.	0		0	n.d.	95	−15	47	n.d.
ai-$C_{17:0}$	15	n.d.	0	−28	0	n.d.	37	n.d.	24	n.d.
n-$C_{16:1}$	114	−26	0	−30	0	n.d.	0	n.d.	0	n.d.
n-$C_{18:1}$	130	n.d.	0	n.d.	97	−25	109	−28	120	n.d.
Phytanic acid	0	n.d.	0	n.d.	0	n.d.	197	−16	57	n.d.
17β(H),21β(H)-C_{32}-Hopanoic acid	0	n.d.	0	n.d.	0	n.d.	0	n.d.	1	n.d.
∑ carboxylic acids	2,320		1,397		1,372		3,591		3,303	
∑ lipids	3,348		2,214		1,594		5,179		4,287	

Abbreviations: *ai*, *anteiso*; GDGT, glycerol dialkyl glycerol tetraethers; *i*, *iso*; lc, long chain; n.d., not determined; sc, short chain.

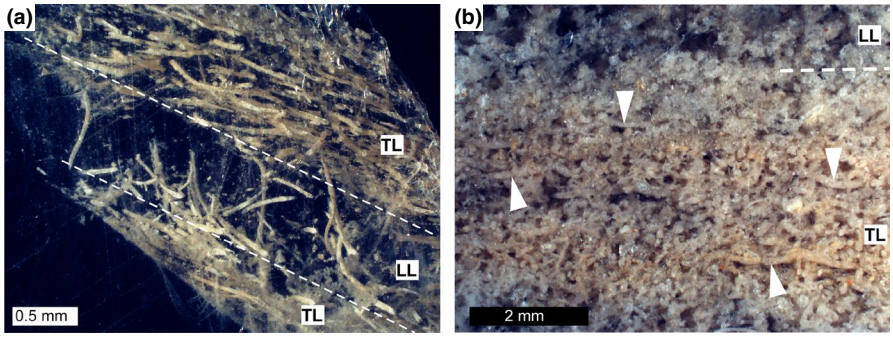

FIGURE 3 Incident light photomicrographs of bottom-grown gypsum with filaments. (a) Close-up of the re-entrant angle of the twinned selenite crystal shown in Figure 2b; note the internal lamination defined by the alternation of limpid (LL) and turbid (TL) laminae. (b) Detail of Figure 2d showing the alternation of darker limpid (LL) and brownish turbid (TL) laminae in stromatolitic gypsum. Note densely packed filamentous fossils in the TL; the white arrows indicate some filaments

FIGURE 4 Transmitted light photomicrographs of filamentous microfossils prevalently entrapped in turbid laminae. (a) Nijar, (b) Monte Tondo, (c–e) hollow filaments in gypsum from Monte Tondo quarry (arrows); (e) UV-light photomicrograph showing an empty filament (arrow) with a fluorescent surface coated by scattered dark non-fluorescent pyrite crystals (white triangles). (f, g) network of filaments in gypsum from Crete (f) and Cyprus (g); the black arrowheads indicate curved filaments. The lamination in (a) and (g) is poorly defined because of high density of filaments

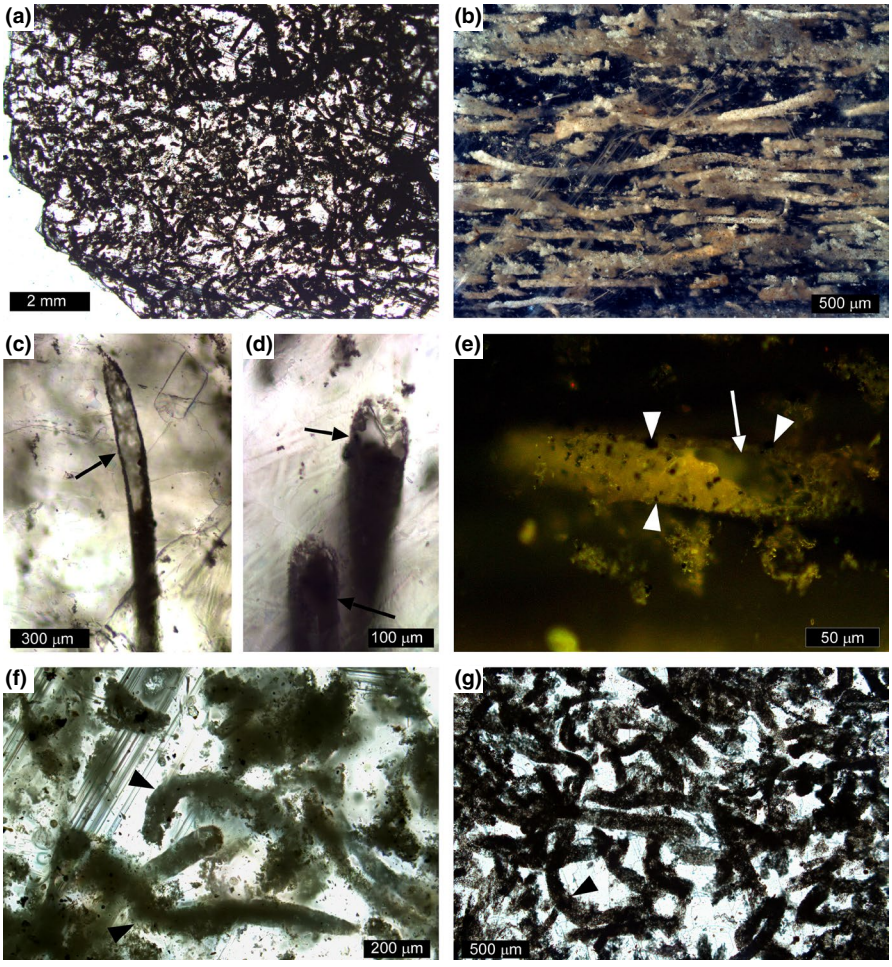

Euryarchaeota (Jebbar et al., 2020; Oren, 2002; Ventosa et al., 2014), and few eukaryotes including the brine shrimp *Artemia salina* and the green alga *Dunaliella salina* (Oren, 2005). Some prokaryotes also live as endoliths in gypsum deposits (Oren et al., 1995; Oren et al., 2009; Stivaletta & Barbieri, 2009; Stivaletta et al., 2010; Jahnke & Des Marais, 2019; Huang et al., 2020). The low biological diversity of modern hypersaline environments is also mirrored by molecular fossil inventories, mostly reflecting input of lipids from halophilic archaea such as DGDs (Dawson et al., 2012; Grice et al., 1998; Turich & Freeman, 2011) and cyanobacteria such as saturated and monounsaturated heptadecanes and heptadecenes (Jahnke et al., 2014). Compared to most modern marine gypsum occurrences (e.g., Jahnke et al., 2014), molecular fossils of the studied Messinian gypsum reflect different ecologies. This difference is probably best explained by the respective depositional environments. While modern gypsum forms in salinas and hypersaline lagoons with water depth at the cm- to m-scale, the primary, bottom-grown Messinian gypsum formed at the seafloor of a marine basin (e.g., Reghizzi et al., 2018).

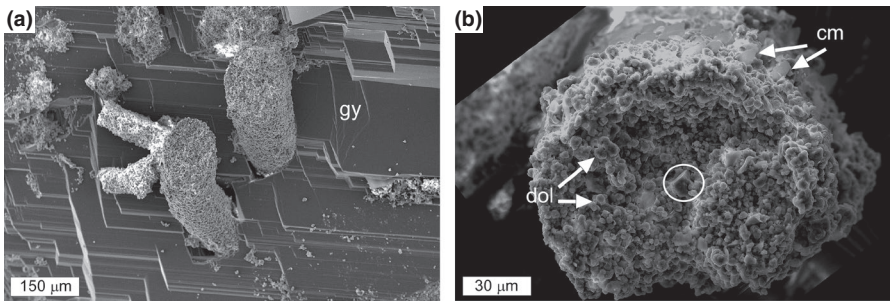

FIGURE 5 Scanning electron microscope photomicrographs. (a) Filamentous structures made mainly of dolomite projecting from gypsum matrix (gy; gypsum was partially dissolved), Monte Tondo. (b) Close-up of one of the filamentous structures with abundant dolomite microcrystals (dol) and clay minerals (cm); celestine crystals are also present (circle), Monte Tondo

A significant input of lipids from planktic biota is not to be expected in case of salterns, salinas, and lagoons.

5.1 | DGDs and GDGTs indicate a diverse aquatic archaeal community

The high contents of $C_{20\text{-}20}$ DGD (archaeol) co-occurring with $C_{20\text{-}25}$ DGD (extended archaeol)—a compound diagnostic of halophilic archaea (Dawson et al., 2012; Teixidor et al., 1993)—in all samples except for Monticino (Figure 6) agree with the presence of a community of halophilic archaea. Archaeol is the major membrane lipid of halophiles (Dawson et al., 2012; Kates, 1993), but is also a common membrane lipid of other archaea, particularly methanogenic and methanotrophic euryarchaea (e.g., Hinrichs et al., 2000; Koga et al., 1998). Other archaeol-producing archaea are marine planktic, mesophilic euryarchaeal groups (e.g., Sollai et al., 2019). Among the potential source organisms of the DGDs extracted from Messinian gypsum, methanotrophic archaea can be excluded, since archaeol (average $\delta^{13}C$ ~ −17‰) does not show the typical $\delta^{13}C$ values of lipids of this group of archaea (as low as −130‰; e.g., Niemann & Elvert, 2008; Himmler et al., 2015) in any of the Messinian gypsum samples. The lowest $\delta^{13}C$ value of archaeol was found for the Monte Tondo sample (−20‰). The fact that this $\delta^{13}C$ value is similar to values of compounds of presumed planktic algal origin (i.e., sterols; −21‰ on average; Figure 6) and values of planktic archaeal origin (i.e., bicyclic and tricyclic biphytanes; −20‰ on average; see below for further discussion) agrees with mesophilic planktic euryarchaea as source of archaeol. The $\delta^{13}C$ values of archaeol from the other sites reflect even less ^{13}C depletion ($\delta^{13}C$ values as high as −14‰, Cyprus). Since extended archaeol exhibits the same $\delta^{13}C$ value like archaeol for all study sites, halophilic euryarchaea, probably planktic, are the most likely producers of both DGDs. Apart from Monte Tondo, $\Delta\delta^{13}C_{DGD\text{-}sterol}$ is as high as +7‰. A similar offset between the lipids of a halophilic archaeal community (DGD producer) and algal phytoplankton (sterol producers) has been described for the late Miocene evaporite-bearing deposits of the Dead Sea Basin (Grice et al., 1998). The observed variability of $\delta^{13}C$ values between halophilic archaea (average $\delta^{13}C$ ~ −17‰) and phytoplankton (−21‰ on average) is in accord with water column stratification, reflecting variations in salinity across the water column. However, the high $\delta^{13}C$ values of the lipids of halophilic archaea in such settings are not yet fully understood (Birgel et al., 2014; Grice et al., 1998). The large $\Delta\delta^{13}C_{DGD\text{-}sterol}$ could be possibly explained by the heterotrophic lifestyle of halophilic archaea, involving the uptake of relatively ^{13}C-enriched carbon from carbohydrates and proteins by halophilic archaea in contrast to photoautotrophic algae assimilating dissolved carbon dioxide (Oren, 1994). Carbohydrates and proteins are generally less ^{13}C-depleted than other organic substrates (e.g., lipids; De Niro and Epstein, 1977, Grice et al., 1998).

Phytanol and the two phytanylglycerol monoethers extracted from Crete and Cyprus gypsum revealed similar $\delta^{13}C$ values (−22 to −13‰) to archaeol and extended archaeol (cf. Birgel et al., 2014; Ziegenbalg et al., 2012); most likely the former compounds represent degradation products of DGDs (cf. Liu et al., 2018). The isoprenoid hydrocarbon phytane, however, is more ^{13}C-depleted ($\delta^{13}C$: −33 to −30‰) than other isoprenoids with phytanyl moieties (Figure 7). Phytane probably derives either from other heterotrophic archaeal communities (Wakeham et al., 2003) or from a secondary, possibly terrigenous source, and is unrelated to the other compounds with phytanyl moieties. To sum up, the lipid biomarker inventory of Messinian gypsum confirms the prominent presence of halophilic archaea in the depositional paleoenvironment—not a surprising result if the gypsum is interpreted as a product of fully hypersaline conditions. Halophilic archaea are commonly thriving in high salinity environments like in some modern shallow-water microbial mats (Bühring et al., 2009; Jahnke et al., 2014). However, uncultured members of the genus *Halobacteria* have also been recognized in aquatic systems with low salt concentrations such as at sulfur-rich springs (Elshahed et al., 2004), estuaries (Purdy et al., 2004; Singh et al., 2010), and the Black Sea, where the salinity of bottom waters is *ca*. 20 PSU (Jessen et al., 2016). In the latter environment, *Halobacteria* were found in sediments covering *Beggiatoa*-dominated microbial mats, occurring where the chemocline intercepts the sea floor and steep gradients of molecular oxygen and hydrogen sulfide exist. According to this example, sulfur-rich microenvironments may have also favored the proliferation of halophilic archaea (cf. Elshahed et al., 2004) in low salinity waters (i.e., with low contents of Na^+ and Cl^- ions) during Messinian gypsum formation (cf. Natalicchio et al., 2014; Evans et al., 2015; see paragraph 5.3).

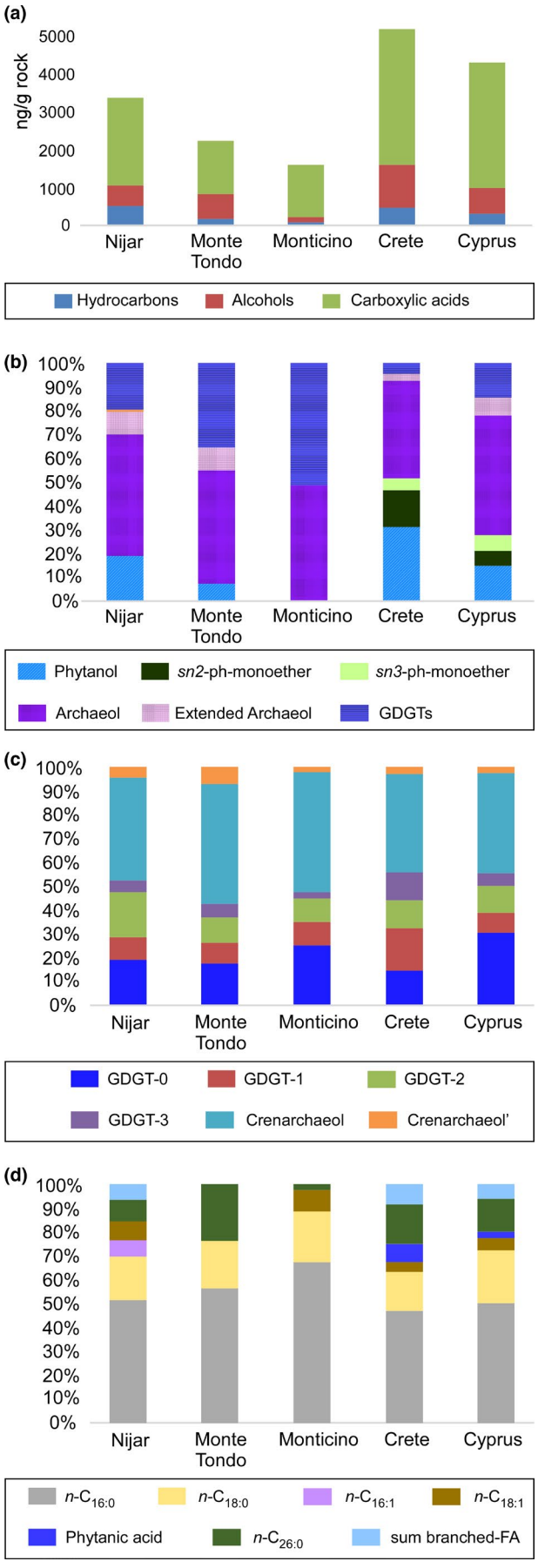

FIGURE 6 (a) Compound distribution in the different fractions of molecular fossils from gypsum in ng/g rock. (b) Relative percentages of isoprenoid alcohols. (c) Relative percentages of glycerol dibiphytanyl glycerol tetraethers (GDGTs). (d) Relative percentages of carboxylic acids (FA, fatty acids)

The observed GDGT assemblages are much different from those reported for modern shallow-water hypersaline settings (Petrick et al., 2019). Halophilic archaea are not known to produce GDGTs (Schouten et al., 2013; Teixidor et al., 1993). Although methanogens isolated from hypersaline lakes have been shown to produce GDGT-0 and GDGT-1, they do not produce extended archaeol (Bale et al., 2019). Most of the GDGTs found in marine sediments are thought to be produced by planktic, ammonia-oxidizing Thaumarchaeota (Brochier-Armanet et al., 2008; Könneke et al., 2005; Schouten et al., 2013; Spang et al., 2010; Wuchter et al., 2006). Crenarchaeol, which is the most abundant GDGT in the studied Messinian gypsum (Figure 5c), is also the predominant GDGT of Thaumarchaeota in the marine epipelagic realm (Schouten et al., 2013; Turich et al., 2007). It is also produced by soil-dwelling Thaumarchaeota (Sinninghe Damsté et al., 2012) and occurs in marine hydrothermal settings (Pearson et al., 2004; De La Torre et al., 2008). In contrast to soil-dwelling Thaumarchaeota, marine Thaumarchaeota produce not only crenarchaeol, but also the acyclic GDGT-0 (caldarchaeol) and minor amounts of cyclopentane ring containing GDGTs (GDGT-1 to GDGT-4). Interestingly, the Messinian gypsum shows a GDGT-distribution similar to that of marine Thaumarchaeota from the modern Mediterranean Sea (Besseling et al., 2019). A derivation of GDGTs from marine Thaumarchaeota also agrees with the GDGT-0/crenarchaeol ratios ranging from 0.4 and 0.7, similar to ratios reported for modern open marine environments (0.5 to 1; Zhang et al., 2016; Petrick et al., 2019). In modern (Słowakiewicz et al., 2016) and ancient (Cheng et al., 2017) hypersaline settings, on the other hand GDGTs are scarce and mostly dominated by GDGT-0.

The $\delta^{13}C$ values of biphytanes found in the Monte Tondo and Cyprus samples help to constrain the sources of (1) caldarchaeol, mostly yielding acyclic biphytanes (BP0) after ether cleavage, and (2) crenarchaeol, the probably source of tricyclic biphytane (BP3) after ether cleavage. The monocyclic (BP1) and bicyclic (BP2) biphytanes derive from GDGTs 1 to 3 and crenarchaeol (BP2 only). The $\delta^{13}C$ values of BP3 (*ca.* −20‰ on average) agree with crenarchaeol deriving from marine autotrophic Thaumarchaeota, an isotopic composition close to that found in modern oceans (*ca.* −21‰; Schouten et al., 2013). The negative $\delta^{13}C$ values of BP0 (as low as −37‰), on the other hand, point to a different source of caldarchaeol, including heterotrophic, possibly benthic archaeal communities (cf. Hoffmann-Sell et al., 2011; Pearson et al., 2016; Wakeham et al., 2003). The former presence of benthic archaea in addition to planktic archaea is supported by relatively high contents of GDGT-1 (up to 18%, Crete) and GDGT-2 (up to 18%, Nijar) compared to modern marine GDGT distributions; these compounds are less abundant in marine planktic archaea (<10% of total GDGTs; Lipp & Hinrichs, 2009). The phylogenetic affiliation of benthic archaea cannot be determined

with certainty, yet methanotrophic archaea can be excluded since this clade reveals different GDGT patterns with the predominance of GDGT-2, ^{13}C depletion, and other isoprenoids not observed in the Messinian gypsum (Birgel et al., 2006, 2008; Natalicchio et al., 2012). A possible group from which the ^{13}C-depleted biphytanes could derive are methanogenic euryarchaea (Hoffmann-Sell et al., 2011; Koga et al., 1998). Among other factors, the isotope composition of lipids synthesized by methanogens depends largely on the metabolized substrate (Londry et al., 2008). Unfortunately, the isotopic composition of GDGT-derived biphytanes has not yet been determined in culture experiments with methanogens. Since archaeol, interpreted to be derived from halophilic archaea, yielded $\delta^{13}C$ values that are 15 to 20‰ higher than the values of acyclic and monocyclic biphytanes, an origin of the latter compounds from halophiles can be excluded—an interpretation in accord with the known compound inventories of halophiles.

To sum up, the lipid inventory of Messinian gypsum suggests the former presence of three archaeal communities including (1) halophiles typified by relatively ^{13}C-enriched DGDs and phytanyl monoethers, (2) planktic thaumarchaea yielding crenarchaeol ($\delta^{13}C$: *ca.* −20‰), and (3) a group of probably benthic archaea producing ^{13}C-depleted GDGT-0 and the cyclic GDGTs 1 and 2. Such high archaeal diversity is not observed in modern shallow-water hypersaline environments (Słowakiewicz et al., 2016; Petrick et al., 2019) and rather agrees with a relatively deep stratified marine basin (Christeleit et al., 2015; García-Veigas et al., 2018). The planktic thaumarchaeal community is believed to have lived in the upper water column, probably typified by diluted marine conditions (Grothe et al., 2020; Natalicchio et al., 2014; Reghizzi et al., 2018), whereas the halophiles inhabited the deeper, more saline part of the water column. Such interpretation is supported by the presence of tetrahymanol in the Cyprus and Crete samples, a proxy of water column stratification (Sinninghe-Damsté et al., 1995; Natalicchio et al., 2017; Sabino et al., 2021).

5.2 | The affiliation of filamentous microfossils

The affiliation of the superabundant filamentous microfossils preserved in Messinian gypsum has not yet been resolved with certainty. At first, they were interpreted to represent fecal pellets of brine shrimps (Schreiber and Decima, 1976), and later, they were assigned to algae (Vai & Ricci Lucchi, 1977), cyanobacteria (Panieri et al., 2010; Rouchy and Monty, 2000) or sulfide-oxidizing bacteria (Dela Pierre et al., 2015; Schopf et al., 2012). An attribution to fecal pellets does not agree with the partial hollowness of the studied filaments (Figure 4e). Hollowness is not expected in fecal pellets, but is strong evidence of a microbial origin of the filamentous microfossils (Andreetto et al., 2019, and reference therein). Such origin is in accord with the curved shape of filaments and their internal segmentation (Dela Pierre et al., 2015). The most striking argument for an assignment to cyanobacteria was the extraction of 16*S r*RNA from samples of the Vena del Gesso gypsum, matching with several cyanobacterial clones and in particular with those of the genus *Geitlerinema*, typical of coastal shallow marine environments (Panieri et al., 2010). The finding of genetic material in several million-year-old geological samples requires excellent preservation of organic matter, supposably caused by early permineralization in gypsum prior to cell decay and disintegration (cf. Schopf et al., 2012). Molecular fossils, which are much more stable than 16*S r*RNA, should therefore confirm the suggested cyanobacterial origin of filaments. Cyanobacteria synthesize lipid biomarkers (Table 3), including diplopterol (Bühring et al., 2009; Rohmer et al., 1984) and bacteriohopanepolyols (Jahnke et al., 2004; Summons et al., 1999; Talbot et al., 2008). Other diagnostic cyanobacterial lipids are short-chain *n*-alkanes, but especially heptadecane and heptadecenes, as well as methylated hepta- and octadecanes (Birgel et al., 2015; Hefter et al., 1993; Jahnke et al., 2014; Kozlowski et al., 2018; Wieland et al., 2008). Some of these compounds or their degradation products tend to be preserved for millions of years in the geological record (Heindel et al., 2015; Summons et al., 1999). Among these cyanobacterial biomarkers, only *n*-C_{17}-alkane (heptadecane) is present in the studied Messinian gypsum (Table 3), yet with moderate contents only, accounting on average for 7% of the total hydrocarbon fraction and corresponding to *n*-C_{17}/*n*-C_{18} ratios below 1. In cyanobacterial mats from modern hypersaline environments, *n*-C_{17} accounts for approximately 80% of the total hydrocarbon fraction and the *n*-C_{17}/*n*-C_{18} ratio is significantly above 1 (e.g., Bühring et al., 2009; Jahnke et al., 2004). Despite heptadecanes being prone to degradation (Hefter et al., 1993; Wieland et al., 2008), in cases of 16*S r*RNA preservation, these cyanobacterial-derived hydrocarbons should be present as well. Although such negative evidence can obviously not exclude the presence of cyanobacteria in the Messinian depositional environment, the scarcity of cyanobacterial biomarkers (see Table 3) renders unlikely an assignment of the superabundant filamentous microfossils to cyanobacteria.

The other previously suggested hypothesis is that the interwoven filaments in the Messinian gypsum represent the remains of colorless sulfide-oxidizing bacteria like *Beggiatoa* and *Thioploca* (Dela Pierre et al., 2015; Schopf et al., 2012). Microbial mats dominated by these large prokaryotes are found in coastal upwelling areas (Arning et al., 2008; Bailey et al., 2009), in stratified basins (e.g., the Black Sea; Jessen et al., 2016), as well as in sulfide-rich marine sediments associated with methane seepage (Knittel et al., 2003; Zhang et al., 2005). The lipid biomarker inventory of mats of sulfide-oxidizing bacteria is typified by high contents of saturated ($C_{16:0}$ and $C_{18:0}$) and monounsaturated ($C_{16:1}$ and $C_{18:1}$) fatty acids (Arning et al., 2008; Jacq et al., 1989; Jiang et al., 2012; McCaffrey et al.,1989; Zhang et al., 2005). The high abundance of these compounds in the majority of the studied Messinian samples is consistent with this hypothesis (Table 3). Unfortunately, other organisms including many bacteria (Elvert et al., 2003; Londry et al., 2004) and diverse phytoplankton (Viso & Marty, 1993; Wakeham, 1995) are known to produce these largely unspecific fatty acids too.

Given the low specificity of the lipids synthesized by sulfide-oxidizing bacteria (Arning et al., 2008), the origin of the filaments can be assessed further with the overall lipid assemblage and the

TABLE 3 Typical lipids produced by chemotrophic sulfide-oxidizing bacteria (= sulfur bacteria) and cyanobacteria and their abundance in Messinian gypsum

	Compounds	Abundance	References	This study
Sulfur bacterial lipids	$C_{16:0}$–$C_{18:0}$ FA	+++	Jacq et al., 1989; McCaffrey et al.,1989; Zhang et al., 2005; Arning et al., 2008; Jiang et al., 2012	+++
	$C_{16:1}$–$C_{18:1}$ FA	+++	Jacq et al., 1989; McCaffrey et al.,1989; Zhang et al., 2005; Arning et al., 2008; Jiang et al., 2012	+
Cyanobacterial lipids	*n*-heptadecane (C_{17})	+++	Hefter et al., 1993; Wieland et al., 2008; Jahnke et al., 2014; Birgel et al., 2015; Kozlowski et al., 2018	
	n-heptadecene ($C_{17:1}$)	+++	Hefter et al., 1993; Wieland et al., 2008; Jahnke et al., 2014; Birgel et al., 2015; Kozlowski et al., 2018	+
	Me-$C_{17;}$ Me-$C_{17:1}$	+	Hefter et al., 1993; Wieland et al., 2008; Jahnke et al., 2014; Birgel et al., 2015; Kozlowski et al., 2018	–
	n-octadecane (C_{18})	++	Hefter et al., 1993; Jahnke et al., 2014	+
	Me-C_{18}	+	Hefter et al., 1993; Jahnke et al., 2014	–
	Diplopterol	+++	Rohmer et al., 1984; Bühring et al., 2009	–
	Bacteriohopanepolyols	+++	Summons et al., 1999; Jahnke et al., 2004; Talbot et al., 2008	–

Note: Abundances: (+++), high; (++), moderate; (+), low; and (–), not detected.
Abbreviations: FA, fatty acids; Me, methyl.

carbon stable isotope patterns. Compounds synthesized by sulfate-reducing bacteria such as *iso*- and *anteiso*-$C_{15:0}$ and $C_{17:0}$ fatty acids (Kaneda, 1991; Perry et al., 1979; Taylor & Parkes, 1983) are present in gypsum from Nijar, Crete, and Cyprus. In the case of Cyprus and Crete gypsum, which are the samples with the highest total lipid abundance (Table 2), even a MAGE—a biomarker of sulfate-reducing bacteria (Grossi et al., 2015; Rütters et al., 2001; Ziegenbalg et al., 2012)—is present despite the generally low stability of MAGEs (Vinçon-Laugier et al., 2018). The relatively high $\delta^{13}C$ value of the MAGE (−17‰) is similar to the value of the *iso*-C_{17} fatty acid (−15‰; Crete), agreeing with the assignment of both compounds to a common source. On the contrary, the lower values (average −26‰) of saturated ($C_{16:0}$ and $C_{18:0}$) and monounsaturated ($C_{16:1}$ and $C_{18:1}$) fatty acids suggest a different source than sulfate-reducing bacteria. Moreover, the $\delta^{13}C$ values of saturated and unsaturated fatty acids in the Messinian gypsum are different from values of lipids deriving from terrestrial plants (e.g., long-chain *n*-alkanes), which are on average more ^{13}C-depleted (−30‰). Compounds deriving from phytoplankton (dinosterol, cholesterol, cholestanol; Volkman, 2003) are less ^{13}C-depleted (average −21‰; Figure 7) on the other hand. Consequently, a predominant origin of these fatty acids from terrestrial plants is unlikely. An origin from phytoplankton is instead possible, since culture experiments revealed that the offset between the $\delta^{13}C$ values of fatty acids and sterols can be as high as 8‰ (Schouten et al., 1998). Although phytoplankton cannot be excluded as a source of these compounds, we suggest that sulfide-oxidizing bacteria represent the most likely source of the $C_{16:0}$, $C_{18:0,}$ $C_{16:1,}$ and $C_{18:1}$ fatty acids, agreeing with petrographic observations (i.e., hollowness, internal segmentation, and curved shape; Andreetto et al., 2019; Schopf et al., 2012) and the presence of iron sulfide inclusions in the filamentous fossils (Figure 4e). Such inclusions can represent the product of early diagenetic transformations of sulfur globules stored within the cells (Dela Pierre et al., 2015), which is a clade diagnostic feature of colorless sulfide-oxidizing bacteria (Schulz & Jørgensen, 2001). Interestingly, a tight association of sulfide-oxidizing bacteria with sulfate-reducing bacteria, as suggested by the biomarker inventory of some of the Messinian gypsum, has been reported for different modern environments (e.g., Arning et al., 2008; Fukui et al., 1999; SamKamaleson et al., 2021).

5.3 | Paleoenvironmental implications

Provided that the assignment of the filamentous fossils to benthic sulfide-oxidizing bacteria like *Beggiatoa* and *Thioploca* is correct and given the association of filamentous body fossils with molecular fossils of sulfate-reducing bacteria—especially in the samples with the highest total lipid contents (i.e., Nijar, Cyprus and Crete)—the basin floor where the Messinian gypsum grew was covered by a benthic assemblage of chemotrophic bacteria involved in an intense sulfur cycle. Such interpretation suggests suboxic to anoxic bottom water conditions and production of hydrogen sulfide through intense bacterial sulfate reduction, in turn sustaining sulfide-oxidizing bacteria (cf. Bailey et al., 2009; Teske et al., 2009). Sulfate-reducing bacteria live in suboxic to anoxic environments, using low molecular weight organic compounds or molecular hydrogen as electron donors (Grossi et al., 2015; Vinçon-Laugier et al., 2016). In case of the Messinian depositional environment, the electron donor was probably a mixture of organic substrates deriving from (1) phytoplankton (diatoms, dinoflagellates) and (2) planktic archaea. The circumstance that the $\delta^{13}C$ values of the MAGE (average *ca.* −17‰; Cyprus and Crete) are similar to those of archaeal-derived compounds (archaeol

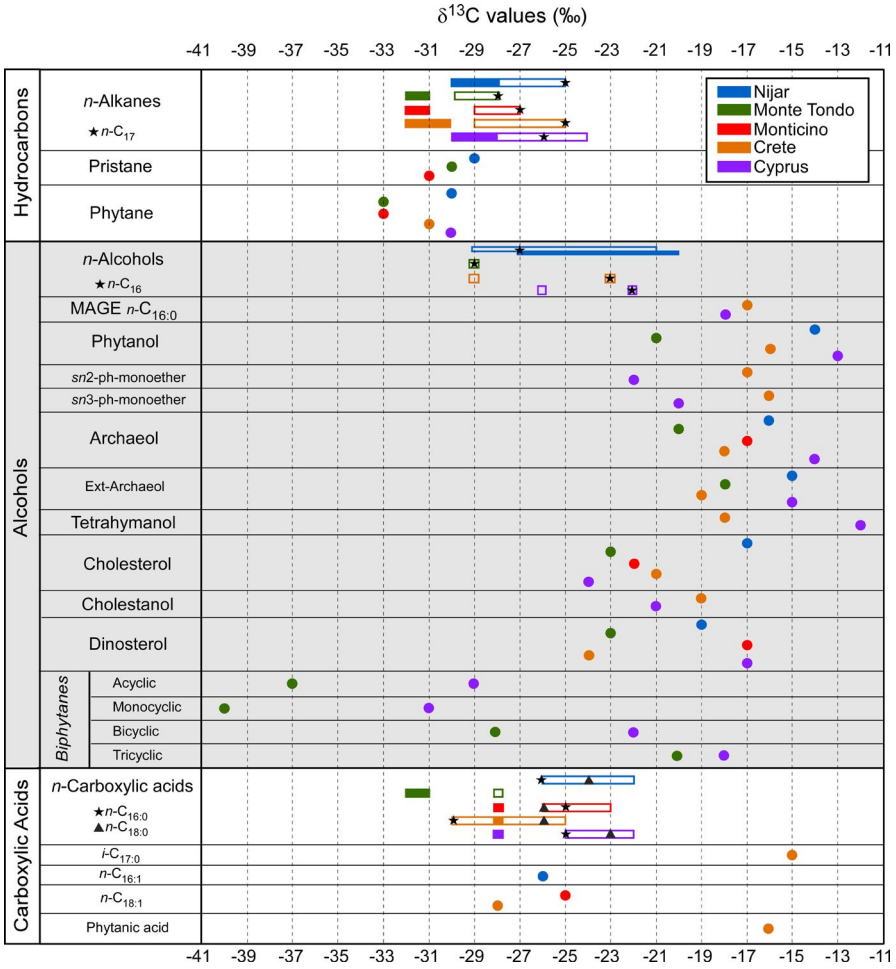

FIGURE 7 Compound-specific $\delta^{13}C$ values (‰ *vs.* V-PDB) of biomarkers from gypsum. For *n*-alkanes, *n*-alcohols, and *n*-carboxylic acids, filled and empty bars indicate the range of values for long-chain (carbon atoms >26) and short-chain (carbon atoms <21) compounds, respectively. *i*, *iso*

and *sn*2/*sn*3-phytanyl monoethers) is in favor of sulfate-reducing bacteria metabolizing low molecular weight compounds deriving from archaeal biomass. This hypothesis is in line with recent studies of the Dead Sea, where bacteria have been found to develop strategies involving the recycling of archaeal necromass (Thomas et al., 2019), which represents the most abundant organic carbon source in this saline basin (Oren, 1999).

The precipitation of gypsum probably caused the rapid entrapment of the benthic assemblage of microbial filaments. The paleoenvironmental conditions behind the formation of the Messinian gypsum are still discussed (e.g., García-Veigas et al., 2018; Grothe et al., 2020; Natalicchio et al., 2014). Data from fluid inclusions in bottom-grown selenitic gypsum challenged the idea that gypsum formed from hypersaline brines resulting from seawater evaporation. Instead, these data indicated that gypsum formed from low salinity waters (i.e., with low contents of Na^+ and Cl^- ions) equivalent to 1.6 wt% sodium chloride on average (Costanzo et al., 2019; Evans et al., 2015; Natalicchio et al., 2014). The water masses probably represented a mixture of marine water, freshwater from Mediterranean rivers (Reghizzi et al., 2018), and brackish water from the Paratethys (Grothe et al., 2020). Interestingly, studies on modern gypsum suggest the involvement of prokaryotes in gypsum formation (van Driessche et al., 2019; Lepinay et al., 2018; Mansor et al., 2018; Thompson & Ferris, 1990). In particular, the oxidation of reduced sulfur species by sulfide-oxidizing bacteria may supply, at least in part, the sulfate needed for gypsum precipitation (e.g., Lepinay et al., 2018; Mansor et al., 2018). Such microbial oxidation has been suggested to promote gypsum supersaturation in bottom waters and to favor the formation of gypsiferous thrombolites in a hypersaline lagoon in Venezuela (Petrash et al., 2012). Since we interpret the fossilized filaments in Messinian gypsum as the remains of sulfide-oxidizing bacteria, a possible microbial involvement in gypsum precipitation should be taken into account in future studies.

6 | CONCLUSIONS

Primary Messinian bottom-grown gypsum deposits, formed during the first stage of the MSC (5.97–5.60 Ma), preserve biosignatures of ancient microbial communities, including diverse molecular fossils and mazes of filamentous microfossils. The molecular fossil assemblages of gypsum from different Mediterranean subbasins are unlike typical assemblage of modern marine gypsum deposits forming in shallow-water hypersaline settings. The abundance of lipids of planktic halophilic archaea, planktic thaumarchaea, and a poorly constrained community of benthic archaea confirms that gypsum formed in a stratified basin typified by a normal marine to diluted upper water column and more saline deeper waters. Petrographic

and mineralogical observations, the overall biomarker inventories, and compound-specific carbon stable isotope patterns agree best with the interpretation that the superabundant filamentous microfossils enclosed in Messinian gypsum are the remains of sulfide-oxidizing bacteria. Sulfide-oxidizing bacteria and sulfate-reducing bacteria were probably the main constituents of chemotrophic microbial mats on the Messinian seafloor.

ACKNOWLEDGMENTS

We thank Jean Marie Rouchy (Paris) for providing gypsum samples from Spain, Crete, and Cyprus as well as for comments on the manuscript. Sebastian Flotow (Bremen) is acknowledged for thin section preparation and Gesine Mollenhauer and Ralph Kreutz (Bremen) for support during GDGT analysis. This research was supported by a Back-to-Research-Grant-2013 of the Faculty of Earth Sciences, Geography and Astronomy, University of Vienna to S.Z. and the Deutsche Forschungsgemeinschaft through the international graduate college EUROPROX (L.H.-S.). The article is further based upon work from COST Action "Uncovering the Mediterranean salt giant" (MEDSALT) supported by COST (European Cooperation in Science and Technology). This project has received funding from the European Union's Horizon 2020 research and innovation program under the Marie Skłodowska-Curie Grant Agreement No. 765256. Comments by Subject Editor Jake Bailey and two anonymous reviewers helped improve the manuscript.

CONFLICT OF INTEREST

The authors declare that there is no conflict of interest regarding the publication of this article.

DATA AVAILABILITY STATEMENT

All data of this article are available in PANGAEA Data Publisher.

ORCID

Jörn Peckmann https://orcid.org/0000-0002-8572-0060

REFERENCES

Allwood, A. C., Burch, I. W., Rouchy, J. M., & Coleman, M. (2013). Morphological biosignatures in gypsum: Diverse formation processes of Messinian (~6.0 Ma) gypsum stromatolites. *Astrobiology*, *13*, 870–886.

Andreetto, F., Dela Pierre, F., Gibert, L. B., Natalicchio, M., & Ferrando, S. (2019). Potential fossilized sulfide-oxidizing bacteria in the upper Miocene sulfur-bearing limestones from the Lorca Basin (SE Spain): Paleoenvironmental implications. *Frontiers in Microbiology*, *10*, 1–15. https://doi.org/10.3389/fmicb.2019.01031

Aref, M. A. M., & Taj, R. J. A. (2012). Recent analog of gypsified microbial laminites and stromatolites in solar salt works and the Miocene gypsum deposits of Saudi Arabia and Egypt. *Arabian Journal of Geosciences*, *6*, 4257–4269. https://doi.org/10.1007/s12517-012-0684-5

Arning, E. T., Birgel, D., Schulz-Vogt, H. N., Holmkvist, L., Jørgensen, B. B., Larson, A., & Peckmann, J. (2008). Lipid biomarker patterns of phosphogenic sediments from upwelling regions. *Geomicrobiology Journal*, *25*, 69–82. https://doi.org/10.1080/01490450801934854

Bailey, J. V., Orphan, V. J., Joye, S. B., & Corsetti, F. A. (2009). Chemotrophic microbial mats and their potential for preservation in the rock record. *Astrobiology*, *9*, 843–859. https://doi.org/10.1089/ast.2008.0314

Bale, N. J., Sorokin, D. Y., Hopmans, E. C., Koenen, M., Rijpstra, W. I. C., Villanueva, L., Wienk, H., & Sinninghe Damsté, J. S. (2019). New insights into the polar lipid composition of extremely halo(alkali) philic Euryarchaea from hypersaline lakes. *Frontiers in Microbiology*, *10*, 1–24. https://doi.org/10.3389/fmicb.2019.00377

Benison, K. C., & Karmanocky, F. J. (2014). Could microorganisms be preserved in Mars gypsum? Insights from terrestrial examples. *Geology*, *42*, 615–618. https://doi.org/10.1130/G35542.1

Besseling, M. A., Hopmans, E. C., Koenen, M., van der Meer, M. T. J., Vreugdenhil, S., Schouten, S., Sinninghe Damsté, J. S., & Villanueva, L. (2019). Depth-related differences in archaeal populations impact the isoprenoid tetraether lipid composition of the Mediterranean Sea water column. *Organic Geochemistry*, *135*, 16–31. https://doi.org/10.1016/j.orggeochem.2019.06.008

Birgel, D., Elvert, M., Han, X., & Peckmann, J. (2008). ^{13}C-depleted biphytanic diacids as tracers of past anaerobic oxidation of methane. *Organic Geochemistry*, *39*, 152–156. https://doi.org/10.1016/j.orggeochem.2007.08.013

Birgel, D., Guido, A., Liu, X., Hinrichs, K.-U., Gier, S., & Peckmann, J. (2014). Hypersaline conditions during deposition of the Calcare di Base revealed from archaeal di- and tetraether inventories. *Organic Geochemistry*, *77*, 11–21. https://doi.org/10.1016/j.orggeochem.2014.09.002

Birgel, D., Meister, P., Lundberg, R., Horath, T. D., Bontognali, T. R. R., Bahniuk, A. M., & McKenzie, J. A. (2015). Methanogenesis produces strong ^{13}C enrichment in stromatolites of Lagoa Salgada, Brazil: A modern analogue for Palaeo-/Neoproterozoic stromatolites? *Geobiology*, *13*, 245–266.

Birgel, D., Thiel, V., Hinrichs, K.-U., Elvert, M., Campbell, K. A., Reitner, J., Farmer, J. D., & Peckmann, J. (2006). Lipid biomarker patterns of methane-seep microbialites from the Mesozoic convergent margin of California. *Organic Geochemistry*, *37*, 1289–1302. https://doi.org/10.1016/j.orggeochem.2006.02.004

Brochier-Armanet, C., Boussau, B., Gribaldo, S., & Forterre, P. (2008). Mesophilic crenarchaeota: Proposal for a third archaeal phylum, the Thaumarchaeota. *Nature Reviews Microbiology*, *6*, 245–252. https://doi.org/10.1038/nrmicro1852

Bühring, S. I., Smittenberg, R. H., Sachse, D., Lipp, J. S., Golubic, S., Sachs, J. P., Hinrichs, K. U., & Summons, R. E. (2009). A hypersaline microbial mat from the Pacific Atoll Kiritimati: Insights into composition and carbon fixation using biomarker analyses and a ^{13}C-labeling approach. *Geobiology*, *7*, 308–323.

Cheng, Z., Xiao, L., Wang, H., Yang, H., Li, J., Huang, T., Xu, Y. I., & Ma, N. (2017). Bacterial and archaeal lipids recovered from subsurface evaporites of Dalangtan Playa on the Tibetan Plateau and their astrobiological implications. *Astrobiology*, *17*, 1112–1122. https://doi.org/10.1089/ast.2016.1526

Christeleit, E. C., Brandon, M. T., & Zhuang, G. (2015). Evidence for deep-water deposition of abyssal Mediterranean evaporites during the Messinian salinity crisis. *Earth and Planetary Science Letters*, *427*, 226–235. https://doi.org/10.1016/j.epsl.2015.06.060

CIESM (2008). The Messinian salinity crisis from mega-deposits to microbiology. In: F. Briand (Ed.), *A consensus report, in 33ème CIESM Workshop Monographs*, *33* (pp. 1–168). CIESM, 16, bd de Suisse, MC-98000, Monaco.

Costanzo, A., Cipriani, M., Feely, M., Cianflone, G., & Dominici, R. (2019). Messinian twinned selenite from the Catanzaro Trough, Calabria, Southern Italy: field, petrographic and fluid inclusion perspectives. *Carbonates and Evaporites*, *34*, 743–756. https://doi.org/10.1007/s13146-019-00516-0

Dawson, K. S., Freeman, K. H., & Macalady, J. L. (2012). Molecular characterization of core lipids from halophilic archaea grown under different salinity conditions. *Organic Geochemistry*, *48*, 1–8. https://doi.org/10.1016/j.orggeochem.2012.04.003

De La Torre, J. R., Walker, C. B., Ingalls, A. E., Könneke, M., & Stahl, D. A. (2008). Cultivation of a thermophilic ammonia oxidizing archaeon synthesizing crenarchaeol. *Environmental Microbiology*, *10*, 810–818. https://doi.org/10.1111/j.1462-2920.2007.01506.x

De Niro, M. J., & Epstein, S. (1977). Mechanism of carbon isotope fractionation associated with lipid synthesis. *Science*, *197*, 261–263. https://doi.org/10.1126/science.327543

Dela Pierre, F., Natalicchio, M., Ferrando, S., Giustetto, R., Birgel, D., Carnevale, G., Gier, S., Lozar, F., Marabello, D., & Peckmann, J. (2015). Are the large filamentous microfossils preserved in Messinian gypsum colorless sulfide-oxidizing bacteria? *Geology*, *43*, 855–858. https://doi.org/10.1130/G37018.1

Delrieu, B., Rouchy, J. M., & Foucault, A. (1993). La surface d'erosion finimessinienne en Crète centrale (Grèce) et sur le pourtour méditerranéen: Rapports avec la crise de salinité méditerranéenne. *Comptes rendus de l'Académie des sciences. Série 2, Mécanique, Physique, Chimie, Sciences De L'univers, Sciences De La Terre*, *316*, 527–533.

Dupraz, C., Reid, R. P., Braissant, O., Decho, A. W., Norman, R. S., & Visscher, P. T. (2009). Processes of carbonate precipitation in modern microbial mats. *Earth-Science Reviews*, *96*, 141–162. https://doi.org/10.1016/j.earscirev.2008.10.005

Elshahed, M. S., Najar, F. Z., Roe, B. A., Oren, A., Dewers, T. A., & Krumholz, L. R. (2004). Survey of archaeal diversity reveals an abundance of halophilic archaea in a low-salt, sulfide- and sulfur-rich spring. *Applied and Environmental Microbiology*, *70*, 2230–2239.

Elvert, M., Boetius, A., Knittel, K., & Jørgensen, B. B. (2003). Characterization of specific membrane fatty acids as chemotaxonomic markers for sulfate-reducing bacteria involved in anaerobic oxidation of methane. *Geomicrobiology Journal*, *20*, 403–419. https://doi.org/10.1080/01490450303894

Evans, N. P., Turchyn, A. V., Gázquez, F., Bontognali, T. R. R., Chapman, H. J., & Hodell, D. A. (2015). Coupled measurements of $\delta^{18}O$ and δD of hydration water and salinity of fluid inclusions in gypsum from the Messinian Yesares Member, Sorbas Basin (SE Spain). *Earth and Planetary Science Letters*, *430*, 499–510. https://doi.org/10.1016/j.epsl.2015.07.071

Fortuin, A. R., & Krijgsman, W. (2003). The Messinian of the Nijar Basin (SE Spain): Sedimentation, depositional environments and paleogeographic evolution. *Sedimentary Geology*, *160*, 213–242. https://doi.org/10.1016/S0037-0738(02)00377-9

Fukui, M., Teske, A., Aßmus, B., Muyzer, G., & Widdel, F. (1999). Physiology, phylogenetic relationships, and ecology of filamentous sulfate-reducing bacteria (genus *Desulfonema*). *Archives of Micobiology*, *172*, 193–203. https://doi.org/10.1007/s002030050760

García-Veigas, J., Cendón, D. I., Gibert, L., Lowenstein, T. K., & Artiaga, D. (2018). Geochemical indicators in Western Mediterranean Messinian evaporites: Implications for the salinity crisis. *Marine Geology*, *403*, 197–214. https://doi.org/10.1016/j.margeo.2018.06.005

Grice, K., Schouten, S., Nissenbaum, A., Charrach, J., & Sinninghe Damsté, J. S. (1998). Isotopically heavy carbon in the C_{21} to C_{25} regular isoprenoids in halite-rich deposits from the Sdom Formation, Dead Sea Basin, Israel. *Organic Geochemistry*, *28*, 349–359. https://doi.org/10.1016/S0146-6380(98)00006-0

Grossi, V., Mollex, D., Vinçon-Laugier, A., Hakil, F., Pacton, M., & Cravo-Laureau, C. (2015). Mono- and dialkyl glycerol ether lipids in anaerobic bacteria: Biosynthetic insights from the mesophilic sulfate reducer *Desulfatibacillum alkenivorans* PF2803T. *Applied and Environmental Microbiology*, *81*, 3157–3168.

Grothe, A., Andreetto, F., Reichart, G.-J., Wolthers, M., Van Baak, C. G. C., Vasiliev, I., Stoica, M., Sangiorgi, F., Middelburg, J. J., Davies, G. R., & Krijgsman, W. (2020). Paratethys pacing of the Messinian salinity crisis: Low salinity waters contributing to gypsum precipitation? *Earth and Planetary Science Letters*, *532*, 1–12. https://doi.org/10.1016/j.epsl.2019.116029

Hefter, J., Thiel, V., Jenisch, A., Galling, U., Kempe, S., & Michaelis, W. (1993). Biomarker indications for microbial contribution to Recent and Late Jurassic carbonate deposits. *Facies*, *29*, 93–105. https://doi.org/10.1007/BF02536922

Heindel, K., Richoz, S., Birgel, D., Brandner, R., Klügel, A., Krystyn, L., Baud, A., Horacek, M., Mohtat, T., & Peckmann, J. (2015). Biogeochemical formation of calyx-shaped carbonate crystal fans in the subsurface of the Early Triassic seafloor. *Gondwana Research*, *27*, 840–861. https://doi.org/10.1016/j.gr.2013.11.004

Himmler, T., Birgel, D., Bayon, G., Pape, T., Ge, L., Bohrmann, G., & Peckmann, J. (2015). Formation of seep carbonates along the Makran convergent margin, northern Arabian Sea and a molecular and isotopic approach to constrain the carbon isotopic composition of parent methane. *Chemical Geology*, *415*, 102–117. https://doi.org/10.1016/j.chemgeo.2015.09.016

Hinrichs, K.-U., Summons, R. E., Orphan, V., Sylva, S. P., & Hayes, J. M. (2000). Molecular and isotopic analysis of anaerobic methane-oxidizing communities in marine sediments. *Organic Geochemistry*, *31*, 1685–1701. https://doi.org/10.1016/S0146-6380(00)00106-6

Hoffmann-Sell, L., Birgel, D., Arning, E. T., Föllmi, K. B., & Peckmann, J. (2011). Archaeal lipids in Neogene dolomites (Monterey and Sisquoc Formations, California) – Planktic versus benthic archaeal sources. *Organic Geochemistry*, *42*, 593–604. https://doi.org/10.1016/j.orggeochem.2011.04.008

Hsü, K. J., Ryan, W. B., & Cita, M. B. (1973). Late Miocene desiccation of the Mediterranean. *Nature*, *242*, 240–244. https://doi.org/10.1038/242240a0

Huang, W., Ertekin, E., Wang, T., Cruz, L., Dailey, M., DiRuggiero, J., & Kisailus, D. (2020). Mechanism of water extraction from gypsum rock by desert colonizing microorganisms. *Proceedings of the National Academy of Sciences of the United States of America*, *117*, 10681–10687. https://doi.org/10.1073/pnas.2001613117

Jacq, E., Prieur, D., Nichols, P., White, D. C., Porter, T., & Geesey, G. G. (1989). Microscopic examination and fatty acid characterization of filamentous bacteria colonizing substrata around subtidal hydrothermal vents. *Archives of Microbiology*, *152*, 64–71. https://doi.org/10.1007/BF00447013

Jahnke, L. L., & Des Marais, D. J. (2019). Carbon isotopic composition of lipid biomarkers from an endoevaporitic gypsum crust microbial mat reveals cycling of mineralized organic carbon. *Geobiology*, *17*, 643–659. https://doi.org/10.1111/gbi.12355

Jahnke, L. L., Embaye, T., Hope, J., Turk, K. A., Van Zuilen, M., Des Marais, D. J., Farmer, J. D., & Summons, R. E. (2004). Lipid biomarker and carbon isotopic signatures for stromatolite-forming, microbial mat communities and Phormidium cultures from Yellowstone National Park. *Geobiology*, *2*, 31–47. https://doi.org/10.1111/j.1472-4677.2004.00021.x

Jahnke, L. L., Turk-Kubo, K. A., N. Parenteau, M., Green, S. J., Kubo, M. D., Vogel, M., Summons, R. E., & Des Marais, D. J. (2014). Molecular and lipid biomarker analysis of a gypsum-hosted endoevaporitic microbial community. *Geobiology*, *12*, 62–82. https://doi.org/10.1111/gbi.12068

Jebbar, M., Hickman-Lewis, K., Cavalazzi, B., Taubner, R. S., Rittmann, S. K. M. R., & Antunes, A. (2020). Microbial diversity and biosignatures: An icy moons perspective. *Space Science Reviews*, *216*, 1–47. https://doi.org/10.1007/s11214-019-0620-z

Jessen, G. L., Lichtschlag, A., Struck, U., & Boetius, A. (2016). Distribution and composition of thiotrophic mats in the hypoxic zone of the Black Sea (150–170 m water depth, Crimea margin). *Frontiers in Microbiology*, *7*, 1–14. https://doi.org/10.3389/fmicb.2016.01011

Jiang, L., Cai, C. F., Zhang, Y. D., Mao, S. Y., Sun, Y. G., Li, K. K., Xiang, L., & Zhang, C. M. (2012). Lipids of sulfate-reducing bacteria and sulfur-oxidizing bacteria found in the Dongsheng uranium deposit. *Chinese Science Bulletin*, *57*, 1311–1319. https://doi.org/10.1007/s11434-011-4955-4

Kaneda, T. (1991). Iso- and anteiso-fatty acids in bacteria: Biosynthesis, function, and taxonomic significance. *Microbiological Reviews*, *55*, 288–302. https://doi.org/10.1128/mr.55.2.288-302.1991

Kates, M. (1993). Membrane lipids of extreme halophiles: biosynthesis, function and evolutionary significance. *Experientia*, *49*, 1027–1036.

Knittel, K., Boetius, A., Lemke, A., Eilers, H., Lochte, K., Pfannkuche, O., Linke, P., & Amann, R. (2003). Activity, distribution, and diversity of sulfate reducers and other bacteria in sediments above gas hydrate (Cascadia margin, Oregon). *Geomicrobiology Journal*, *20*, 269–294. https://doi.org/10.1080/01490450303896

Koga, Y., Morii, H., Akagawa-Matsushita, M., & Ohga, I. (1998). Correlation of polar lipid composition with 16S rRNA phylogeny in methanogens. Further analysis of lipid components. *Bioscience, Biotechnology and Biochemistry*, *62*, 230–236.

Könneke, M., Bernhard, A. E., de la Torre, J. R., Walker, C. B., Waterbury, J. B., & Stahl, D. A. (2005). Isolation of an autotrophic ammonia-oxidizing marine archaeon. *Nature*, *437*, 543–546. https://doi.org/10.1038/nature03911

Kozlowski, J. A., Johnson, M. E., Ledesma-Vazquez, J., Birgel, D., Peckmann, J., & Schleper, C. (2018). Microbial diversity of a closed salt lagoon in the Puertecitos area, Upper Gulf of California. *Ciencias Marinas*, *44*, 71–90. https://doi.org/10.7773/cm.v44i2.2825

Krijgsman, W., Blanc-Valleron, M.-M., Flecker, R., Hilgen, F. J., Kouwenhoven, T. J., Merle, D., Orszag-Sperber, F., & Rouchy, J.-M. (2002). The onset of the Messinian salinity crisis in the Eastern Mediterranean (Pissouri Basin, Cyprus). *Earth and Planetary Science Letters*, *194*, 299–310. https://doi.org/10.1016/S0012-821X(01)00574-X

Lepinay, C., Mihajlovski, A., Touron, S., Seyer, D., Bousta, F., & Di Martino, P. (2018). Bacterial diversity associated with saline efflorescences damaging the walls of a French decorated prehistoric cave registered as a World Cultural Heritage Site. *International Biodeterioration and Biodegradation*, *130*, 55–64. https://doi.org/10.1016/j.ibiod.2018.03.016

Lipp, J. S., & Hinrichs, K.-U. (2009). Structural diversity and fate of intact polar lipids in marine sediments. *Geochimica et Cosmochimica Acta*, *73*, 6816–6833. https://doi.org/10.1016/j.gca.2009.08.003

Liu, X.-L., Birgel, D., Elling, F. J., Sutton, P. A., Lipp, J. S., Zhu, R., Zhang, C., Könneke, M., Peckmann, J., Rowland, S. J., Summons, R. E., & Hinrichs, K.-U. (2016). From ether to acid: A plausible degradation pathway of glycerol dialkyl glycerol tetraethers. *Geochimica et Cosmochimica Acta*, *183*, 138–152. https://doi.org/10.1016/j.gca.2016.04.016

Liu, X. L., Lipp, J. S., Birgel, D., Summons, R. E., & Hinrichs, K.-U. (2018). Predominance of parallel glycerol rearrangement in archaeal tetraethers from marine sediments: Structural features revealed from degradation products. *Organic Geochemistry*, *115*, 12–23.

Londry, K. L., Dawson, K. G., Grover, H. D., Summons, R. E., & Bradley, A. S. (2008). Stable carbon isotope fractionation between substrates and products of *Methanosarcina barkeri*. *Organic Geochemistry*, *39*, 608–621. https://doi.org/10.1016/j.orggeochem.2008.03.002

Londry, K. L., Jahnke, L. L., & Des Marais, D. J. (2004). Stable carbon isotope ratios of lipid biomarkers of sulfate-reducing bacteria. *Applied and Environmental Microbiology*, *70*, 745–751. https://doi.org/10.1128/AEM.70.2.745-751.2004

Lu, F. H. (2006). Lithofacies and water-body record of Messinian evaporites in Nijar Basin, SE Spain. *Sedimentary Geology*, *188–189*, 115–130. https://doi.org/10.1016/j.sedgeo.2006.03.001

Lu, F. H., & Meyers, W. J. (2003). Sr, S, and OSO4 isotopes and the depositional environments of the upper Miocene evaporites, Spain. *Journal of Sedimentary Research*, *73*, 444–450. https://doi.org/10.1306/093002730444

Lu, F. H., Meyers, W. J., & Hanson, G. N. (2002). Trace elements and environmental significance of Messinian gypsum deposits, the Nijar Basin, southeastern Spain. *Chemical Geology*, *192*, 149–161. https://doi.org/10.1016/S0009-2541(02)00009-8

Lu, F. H., Meyers, W. J., & Schoonen, M. A. (2001). S and O (SO4) isotopes, simultaneous modeling, and environmental significance of the Nijar Messinian gypsum, Spain. *Geochimica et Cosmochimica Acta*, *65*, 3081–3092. https://doi.org/10.1016/S0016-7037(01)00553-1

Lugli, S., Manzi, V., Roveri, M., & Schreiber, B. C. (2010). The primary lower gypsum in the mediterranean: A new facies interpretation for the first stage of the Messinian salinity crisis. *Palaeogeography, Palaeoclimatology, Palaeoecology*, *297*, 83–99.

Mansor, M., Harouaka, K., Gonzales, M. S., Macalady, J. L., & Fantle, M. S. (2018). Transport-induced spatial patterns of sulfur isotopes ($\delta^{34}S$) as biosignatures. *Astrobiology*, *18*, 59–72.

Manzi, V., Lugli, S., Roveri, M., Dela Pierre, F., Gennari, R., Lozar, F., Natalicchio, M., Schreiber, B. C., Taviani, M., & Turco, E. (2016). The Messinian salinity crisis in Cyprus: A further step towards a new stratigraphic framework for Eastern Mediterranean. *Basin Research*, *28*, 207–236. https://doi.org/10.1111/bre.12107

McCaffrey, M. A., Farrington, J. W., & Repeta, D. J. (1989). Geochemical implications of the lipid composition of *Thioploca* spp. from the Peru upwelling region-15°S. *Organic Geochemistry*, *14*, 61–68. https://doi.org/10.1016/0146-6380(89)90019-3

Natalicchio, M., Birgel, D., Dela Pierre, F., Martire, L., Clari, P., Spötl, C., & Peckmann, J. (2012). Polyphasic carbonate precipitation in the shallow subsurface: Insights from microbially-formed authigenic carbonate beds in upper Miocene sediments of the Tertiary Piedmont Basin (NW Italy). *Palaeogeography, Palaeoclimatology, Palaeoecology*, *329–330*, 158–172. https://doi.org/10.1016/j.palaeo.2012.02.026

Natalicchio, M., Birgel, D., Peckmann, J., Lozar, F., Carnevale, G., Liu, X., Hinrichs, K.-U., & Dela Pierre, F. (2017). An archaeal biomarker record of paleoenvironmental change across the onset of the Messinian salinity crisis in the absence of evaporites (Piedmont Basin, Italy). *Organic Geochemistry*, *113*, 242–253. https://doi.org/10.1016/j.orggeochem.2017.08.014

Natalicchio, M., Dela Pierre, F., Lugli, S., Lowenstein, T. K., Feiner, S. J., Ferrando, S., Manzi, V., Roveri, M., & Clari, P. (2014). Did late Miocene (Messinian) gypsum precipitate from evaporated marine brines? Insights from the Piedmont basin (Italy). *Geology*, *42*, 179–182. https://doi.org/10.1130/G34986.1

Niemann, H., & Elvert, M. (2008). Diagnostic lipid biomarker and stable carbon isotope signatures of microbial communities mediating the anaerobic oxidation of methane with sulphate. *Organic Geochemistry*, *39*, 1668–1677. https://doi.org/10.1016/j.orggeochem.2007.11.003

Omodeo Salé, S., Gennari, R., Lugli, S., Manzi, V., & Roveri, M. (2012). Tectonic and climatic control on the Late Messinian sedimentary evolution of the Nijar Basin (Betic Cordillera, Southern Spain). *Basin Research*, *24*, 314–337. https://doi.org/10.1111/j.1365-2117.2011.00527.x

Oren, A. (1994). The ecology of the extremely halophilic archaea. *FEMS Microbiology Reviews*, *13*, 415–439. https://doi.org/10.1111/j.1574-6976.1994.tb00060.x

Oren, A. (1999). Bioenergetic aspects of halophilism. *Microbiology and Molecular Biology Reviews*, *63*, 334–348. https://doi.org/10.1128/MMBR.63.2.334-348.1999

Oren, A. (2002). Diversity of halophilic microorganisms: Environments, phylogeny, physiology, and applications. *Journal of Microbiology & Biotechnology*, *28*, 56–63.

Oren, A. (2005). A hundred years of *Dunaliella* research: 1905–2005. *Saline Systems*, *1*, 2.

Oren, A., Kuhl, M., & Karsten, U. (1995). An endoevaporitic microbial mat within a gypsum crust: Zonation of phototrophs, photopigments, and light penetration. *Marine Ecology Progress Series*, *128*, 151–159. https://doi.org/10.3354/meps128151

Oren, A., Sørensen, K. B., Canfield, D. E., Teske, A. P., Ionescu, D., Lipski, A., & Altendorf, K. (2009). Microbial communities and processes within a hypersaline gypsum crust in a saltern evaporation pond

(Eilat, Israel). *Hydrobiologia*, *626*, 15–26. https://doi.org/10.1007/s10750-009-9734-8

Orszag-Sperber, F., Caruso, A., Blanc-Valleron, M. M., Merle, D., & Rouchy, J. M. (2009). The onset of the Messinian salinity crisis: Insights from Cyprus sections. *Sedimentary Geology*, *217*, 52–64. https://doi.org/10.1016/j.sedgeo.2009.03.006

Ortí, F. (2011). Selenite facies in marine evaporites: A review. *International Association of Sedimentologists Special Publication*, *43*, 431–464.

Panieri, G., Lugli, S., Manzi, V., Roveri, M., Schreiber, B. C., & Palinska, K. A. (2010). Ribosomal RNA gene fragments from fossilized cyanobacteria identified in primary gypsum from the late Miocene, Italy. *Geobiology*, *8*, 101–111. https://doi.org/10.1111/j.1472-4669.2009.00230.x

Pearson, A., Huang, Z., Ingalls, A. E., Romanek, C. S., Wiegel, J., Freeman, K. H., Smittenberg, R. H., & Zhang, C. L. (2004). Nonmarine crenarchaeol in Nevada hot springs. *Applied and Environmental Microbiology*, *70*, 5229–5237. https://doi.org/10.1128/AEM.70.9.5229-5237.2004

Pearson, A., Hurley, S. J., Walter, S. R. S., Kusch, S., Lichtin, S., & Zhang, Y. G. (2016). Stable carbon isotope ratios of intact GDGTs indicate heterogeneous sources to marine sediments. *Geochimica et Cosmochimica Acta*, *181*, 18–35. https://doi.org/10.1016/j.gca.2016.02.034

Perry, G. J., Volkman, J. K., Johns, R. B., & Bavor, H. J. (1979). Fatty acids of bacterial origin in contemporary marine sediments. *Geochimica et Cosmochimica Acta*, *43*, 1715–1725. https://doi.org/10.1016/0016-7037(79)90020-6

Petrash, D. A., Gingras, M. K., Lalonde, S. V., Orange, F., Pecoits, E., & Konhauser, K. O. (2012). Dynamic controls on accretion and lithification of modern gypsum-dominated thrombolites, Los Roques, Venezuela. *Sedimentary Geology*, *245–246*, 29–47. https://doi.org/10.1016/j.sedgeo.2011.12.006

Petrick, B., Reuning, L., & Martínez-García, A. (2019). Distribution of glycerol dialkyl glycerol tetraethers (GDGTs) in microbial mats from Holocene and Miocene Sabkha sediments. *Frontiers in Earth Science*, *7*, 1–11. https://doi.org/10.3389/feart.2019.00310

Purdy, K. J., Cresswell-Maynard, T. D., Nedwell, D. B., McGenity, T. J., Grant, W. D., Timmis, K. N., & Embley, T. M. (2004). Isolation of haloarchaea that grow at low salinities. *Environmental Microbiology*, *6*, 591–595. https://doi.org/10.1111/j.1462-2920.2004.00592.x

Reghizzi, M., Lugli, S., Manzi, V., Rossi, F. P., & Roveri, M. (2018). Orbitally forced hydrological balance during the Messinian Salinity Crisis: Insights from strontium isotopes ($^{87}Sr/^{86}Sr$) in the Vena del Gesso Basin (Northern Apennines, Italy). *Paleoceanography and Paleoclimatology*, *33*, 716–731.

Rohmer, M., Bouvier-Nave, P., & Ourisson, G. (1984). Distribution of hopanoid triterpenes in prokaryotes. *Journal of General Microbiology*, *130*, 1137–1150.

Rouchy, J. M. (1982). *La Genèse des Évaporites Messiniennes de Méditerranée* (p. 267). Mémoires du Muséum National d'Histoire Naturelle, Série C, Édition du Muséum.

Rouchy, J. M., & Caruso, A. (2006). The Messinian salinity crisis in the Mediterranean basin: A reassessment of the data and an integrated scenario. *Sedimentary Geology*, *188–189*, 35–67. https://doi.org/10.1016/j.sedgeo.2006.02.005

Rouchy, J. M., & Monty, C. L. (1981). Stromatolites and cryptalgal laminites associated with Messinian gypsum of Cyprus. In C. Monty (Ed.), *Phanerozoic stromatolites* (p. 249). Springer.

Rouchy, J. M., & Monty, C. (2000). Gypsum microbial sediments: Neogene and modern examples. In R. E. Riding, & S. M. Awramik (Eds.), *Microbial Sediments* (p. 331). Springer.

Roveri, M., Flecker, R., Krijgsman, W., Lofi, J., Lugli, S., Manzi, V., Sierro, F. J., Bertini, A., Camerlenghi, A., De Lange, G., Govers, R., Hilgen, F. J., Hübscher, C., Meijer, P. T., & Stoica, M. (2014). The Messinian Salinity Crisis: Past and future of a great challenge for marine sciences. *Marine Geology*, *352*, 25–58. https://doi.org/10.1016/j.margeo.2014.02.002

Roveri, M., Lugli, S., Manzi, V., & Schreiber, B. C. (2008). The Messinian Sicilian stratigraphy revisited: New insights for the Messinian salinity crisis. *Terra Nova*, *20*, 483–488. https://doi.org/10.1111/j.1365-3121.2008.00842.x

Rütters, H., Sass, H., Cypionka, H., & Rullkötter, J. (2001). Monoalkylether phospholipids in the sulfate-reducing bacteria *Desulfosarcina variabilis* and *Desulforhabdus amnigenus*. *Archives of Microbiology*, *176*, 435–442. https://doi.org/10.1007/s002030100343

Sabino, M., Dela Pierre, F., Natalicchio, M., Birgel, D., Gier, S., & Peckmann, J. (2021). The response of water column and sedimentary environments to the advent of the Messinian salinity crisis: insights from an onshore deep-water section (Govone, NW Italy). *Geological Magazine*, *158*, 825–841. https://doi.org/10.1017/S0016756820000874

SamKamaleson, A., Gonsalves, M. J., Karthikeyan, A., & LokaBharathi, P. A. (2021). Sulfate-reducing and sulfur-oxidizing bacterial activity in the coastal waters of Arabian Sea during post upwelling season. *Geomicrobiology Journal*, *38*, 150–163. https://doi.org/10.1080/01490451.2020.1818894

Schinteie, R., & Brocks, J. J. (2017). Paleoecology of Neoproterozoic hypersaline environments: Biomarker evidence for haloarchaea, methanogens, and cyanobacteria. *Geobiology*, *15*, 641–663. https://doi.org/10.1111/gbi.12245

Schopf, J. W., Farmer, J. D., Foster, I. S., Kudryavtsev, A. B., Gallardo, V. A., & Espinoza, C. (2012). Gypsum-permineralized microfossils and their relevance to the search for life on Mars. *Astrobiology*, *12*, 619–633. https://doi.org/10.1089/ast.2012.0827

Schouten, S., Hopmans, E. C., & Sinninghe Damsté, J. S. (2013). The organic geochemistry of glycerol dialkyl glycerol tetraether lipids: A review. *Organic Geochemistry*, *54*, 19–61. https://doi.org/10.1016/j.orggeochem.2012.09.006

Schouten, S., Klein Breteler, W. C. M., Blokker, P., Schogt, N., Rijpstra, W. I. C., Grice, K., Baas, M., & Sinninghe Damsté, J. S. (1998). Biosynthetic effects on the stable carbon isotopic compositions of algal lipids: implications for deciphering the carbon isotopic biomarker record. *Geochimica et Cosmochimica Acta*, *62*, 1397–1406. https://doi.org/10.1016/S0016-7037(98)00076-3

Schreiber, B. C., & Decima, A. (1976). Sedimentary facies produced under evaporitic environments: A review. *Memorie Della Società Geologica Italiana*, *16*, 111–126.

Schulz, H. N., & Jørgensen, B. B. (2001). Big bacteria. *Annual Review of Microbiology*, *55*, 105–137. https://doi.org/10.1146/annurev.micro.55.1.105

Singh, S. K., Verma, P., Ramaiah, N., Chandrashekar, A. A., & Shouche, Y. S. (2010). Phylogenetic diversity of archaeal 16S rRNA and ammonia monooxygenase genes from tropical estuarine sediments on the central west coast of India. *Research in Microbiology*, *161*, 177–186. https://doi.org/10.1016/j.resmic.2010.01.008

Sinninghe Damsté, J. S., Rijpstra, W. I. C., Hopmans, E. C., den Uijl, M. J., Weijers, J. W. H., & Schouten, S. (2018). The enigmatic structure of the crenarchaeol isomer. *Organic Geochemistry*, *124*, 22–28. https://doi.org/10.1016/j.orggeochem.2018.06.005

Sinninghe Damsté, J. S., Rijpstra, W. I. C., Hopmans, E. C., Jung, M.-Y., Kim, J.-G., Rhee, S.-K., Stieglmeier, M.-G., & Schleper, C. (2012). Intact polar and core glycerol dibiphytanyl glycerol tetraether lipids of Group I.1a and I.1b Thaumarchaeota in soil. *Applied and Environmental Microbiology*, *78*, 6866–6874.

Sinninghe-Damsté, J. S., Kenig, F., Koopmans, M. P., Köster, J., Schouten, S., Hayes, J. M., & de Leeuw, J. W. (1995). Evidence for gammacerane as an indicator of water column stratification. *Geochimica et Cosmochimica Acta*, *59*, 1895–1900. https://doi.org/10.1016/0016-7037(95)00073-9

Słowakiewicz, M., Whitaker, F., Thomas, L., Tucker, M. E., Zheng, Y., Gedl, P., & Pancost, R. D. (2016). Biogeochemistry of intertidal microbial mats from Qatar: New insights from organic matter

characterisation. *Organic Geochemistry*, *102*, 14–29. https://doi.org/10.1016/j.orggeochem.2016.09.006

Sollai, M., Villanueva, L., Hopmans, E. C., Keil, R. G., & Sinninghe Damsté, J. S. (2019). Archaeal sources of intact membrane lipid biomarkers in the oxygen deficient zone of the eastern tropical south Pacific. *Frontiers in Microbiology*, *10*, 1–20. https://doi.org/10.3389/fmicb.2019.00765

Spang, A., Hatzenpichler, R., Brochier-Armanet, C., Rattei, T., Tischler, P., Spieck, E., Streit, W., Stahl, D. A., Wagner, M., & Schleper, C. (2010). Distinct gene set in two different lineages of ammonia-oxidizing archaea supports the phylum Thaumarchaeota. *Trends in Microbiology*, *18*, 331–340. https://doi.org/10.1016/j.tim.2010.06.003

Stivaletta, N., & Barbieri, R. (2009). Endolithic microorganisms from spring mound evaporite deposits (southern Tunisia). *Journal of Arid Environments*, *73*, 33–39. https://doi.org/10.1016/j.jaridenv.2008.09.024

Stivaletta, N., Łopez-Garćia, P., Boihem, L., Millie, D. F., & Barbieri, R. (2010). Biomarkers of endolithic communities within gypsum crusts (Southern Tunisia). *Geomicrobiology Journal*, *27*, 101–110. https://doi.org/10.1080/01490450903410431

Summons, R. E., Jahnke, L. L., Hope, J. M., & Logan, G. A. (1999). 2-Methylhopanoids as biomarkers for cyanobacterial oxygenic photosynthesis. *Nature*, *400*, 554–557. https://doi.org/10.1038/23005

Talbot, H. M., Summons, R. E., Jahnke, L. L., Cockell, C. S., Rohmer, M., & Farrimond, P. (2008). Cyanobacterial bacteriohopanepolyol signatures from cultures and natural environmental settings. *Organic Geochemistry*, *39*, 232–263. https://doi.org/10.1016/j.orggeochem.2007.08.006

Taylor, J., & Parkes, R. J. (1983). The cellular fatty acids of the sulphate-reducing bacteria, *Desulfobacter* sp., *Desulfobulbus* sp. and *Desulfovibrio desulfuricans*. *Journal of General Microbiology*, *129*, 3303–3309.

Teixidor, P., Grimalt, J. O., Pueyo, J. J., & Rodriguez-Valera, F. (1993). Isopranylglycerol diethers in non-alkaline evaporitic environments. *Geochimica et Cosmochimica Acta*, *57*, 4479–4489. https://doi.org/10.1016/0016-7037(93)90497-K

Teske, A., Jørgensen, B. B., & Gallardo, V. A. (2009). Filamentous bacteria inhabiting the sheaths of marine *Thioploca* spp. on the Chilean continental shelf. *FEMS Microbiology Ecology*, *68*, 164–172. https://doi.org/10.1111/j.1574-6941.2009.00659.x

Thomas, C., Grossi, V., Antheaume, I., & Ariztegui, D. (2019). Recycling of archaeal biomass as a new strategy for extreme life in Dead Sea deep sediments. *Geology*, *47*, 479–482. https://doi.org/10.1130/G45801.1

Thompson, J. B., & Ferris, F. G. (1990). Cyanobacterial precipitation of gypsum, calcite, and magnesite from natural alkaline lake water. *Geology*, *18*, 995–998. https://doi.org/10.1130/0091-7613(1990)018<0995:CPOGCA>2.3.CO;2

Turich, C., & Freeman, K. H. (2011). Archaeal lipids record paleosalinity in hypersaline systems. *Organic Geochemistry*, *42*, 1147–1157. https://doi.org/10.1016/j.orggeochem.2011.06.002

Turich, C., Freeman, K. H., Bruns, M. A., Conte, M., Jones, A. D., & Wakeham, S. G. (2007). Lipids of marine Archaea: Patterns and provenance in the water-column and sediments. *Geochimica et Cosmochimica Acta*, *71*, 3272–3291. https://doi.org/10.1016/j.gca.2007.04.013

Vai, G. B., & Ricci Lucchi, F. (1977). Algal crusts, autochthonous and clastic gypsum in a cannibalistic evaporites basin: a case history from the Messinian of Northern Apennines. *Sedimentology*, *24*, 211–244.

Van de Poel, H. M. (1991). Messinian stratigraphy of the Nijar basin (S.E. Spain) and the origin of its gypsum–ghost limestones. *Geologie En Mijnbouw*, *70*, 215–234.

Van Driessche, A. E. S., Stawski, T. M., & Kellermeier, M. (2019). Calcium sulfate precipitation pathways in natural and engineered environments. *Chemical Geology*, *530*, 1–29. https://doi.org/10.1016/j.chemgeo.2019.119274

Vasiliev, I., Mezger, E. M., Lugli, S., Reichart, G. J., Manzi, V., & Roveri, M. (2017). How dry was the Mediterranean during the Messinian salinity crisis? *Palaeogeography, Palaeoclimatology, Palaeoecology*, *471*, 120–133. https://doi.org/10.1016/j.palaeo.2017.01.032

Ventosa, A., Fernández, A. B., León, M. J., Sánchez-Porro, C., & Rodriguez-Valera, F. (2014). The Santa Pola saltern as a model for studying the microbiota of hypersaline environments. *Extremophiles*, *18*, 811–824. https://doi.org/10.1007/s00792-014-0681-6

Vinçon-Laugier, A., Cravo-Laureau, C., & Grossi, V. (2018). Selective preservation among bacterial alkyl glycerol ether lipid structures during long term oxic and anoxic incubation. *Organic Geochemistry*, *125*, 24–28. https://doi.org/10.1016/j.orggeochem.2018.08.009

Vinçon-Laugier, A., Grossi, V., Pacton, M., Escarguel, G., & Cravo-Laureau, C. (2016). The alkyl glycerol ether lipid composition of heterotrophic sulfate reducing bacteria strongly depends on growth substrate. *Organic Geochemistry*, *98*, 141–154. https://doi.org/10.1016/j.orggeochem.2016.05.015

Viso, A. C., & Marty, J. C. (1993). Fatty acids from 28 marine microalgae. *Phytochemistry*, *34*, 1521–1533. https://doi.org/10.1016/S0031-9422(00)90839-2

Vogel, M. B., Des Marais, D. J., Parenteau, M. N., Jahnke, L. L., Turk, K. A., & Kubo, M. D. Y. (2010). Biological influences on modern sulfates: Textures and composition of gypsum deposits from Guerrero Negro, Baja California Sur, Mexico. *Sedimentary Geology*, *223*, 265–280. https://doi.org/10.1016/j.sedgeo.2009.11.013

Volkman, J. K. (2003). Sterols in microorganisms. *Applied Microbiology and Biotechnology*, *60*, 495–506. https://doi.org/10.1007/s00253-002-1172-8

Wakeham, S. G. (1995). Lipid biomarkers for heterotrophic alteration of suspended particulate organic matter in oxygenated and anoxic water columns of the ocean. *Deep-Sea Research Part I*, *42*, 1749–1771. https://doi.org/10.1016/0967-0637(95)00074-G

Wakeham, S. G., Lewis, C. M., Hopmans, E. C., Schouten, S., & Sinninghe Damsté, J. S. (2003). Archaea mediate anaerobic oxidation of methane in deep euxinic waters of the Black Sea. *Geochimica et Cosmochimica Acta*, *67*, 1359–1374. https://doi.org/10.1016/S0016-7037(02)01220-6

Wieland, A., Pape, T., Möbius, J., Klock, J. H., & Michaelis, W. (2008). Carbon pools and isotopic trends in a hypersaline cyanobacterial mat. *Geobiology*, *6*, 171–186. https://doi.org/10.1111/j.1472-4669.2007.00138.x

Wuchter, C., Abbas, B., Coolen, M. J. L., Herfort, L., van Bleijswijk, J., Timmers, P., Strous, M., Teira, E., Herndl, G. J., Middelburg, J. J., Schouten, S., & Sinninghe Damsté, J. S. (2006). Archaeal nitrification in the ocean. *Proceedings of the National Academy of Sciences of the United States of America*, *103*, 12317–12322. https://doi.org/10.1073/pnas.0600756103

Zhang, C. L., Huang, Z., Cantu, J., Pancost, R. D., Brigmon, R. L., Lyons, T. W., & Sassen, R. (2005). Lipid biomarkers and carbon isotope signatures of a microbial (*Beggiatoa*) mat associated with gas hydrates in the Gulf of Mexico. *Applied and Environmental Microbiology*, *71*, 2106–2112.

Zhang, Y. G., Pagani, M., & Wang, Z. (2016). Ring Index: A new strategy to evaluate the integrity of TEX86 paleothermometry. *Paleoceanography*, *31*, 220–232.

Ziegenbalg, S. B., Birgel, D., Hoffmann-Sell, L., Pierre, C., Rouchy, J. M., & Peckmann, J. (2012). Anaerobic oxidation of methane in hypersaline Messinian environments revealed by ^{13}C-depleted molecular fossils. *Chemical Geology*, *292–293*, 140–148.

How to cite this article: Natalicchio, M., Birgel, D., Dela Pierre, F., Ziegenbalg, S., Hoffmann-Sell, L., Gier, S., & Peckmann, J. (2021). Messinian bottom-grown selenitic gypsum: An archive of microbial life. *Geobiology*, 00, 1–19. https://doi.org/10.1111/gbi.12464